

RESEARCH ARTICLE

This is a PDF file of an article that is not yet the definitive version of record. This version will undergo additional copyediting, typesetting and review before it is published in its final form, but we are providing this version to give early visibility of the article. Please note that, during the production process, errors may be discovered which could affect the content, and all legal disclaimers that apply to the journal pertain. The final authenticated version is available online at: <https://doi.org/10.1093/plcell/koad141>

For the purpose of Open Access, the author has applied a CC BY public copyright licence to any Author Accepted Manuscript version arising from this submission.

Phosphorylation of Arabidopsis ADAPTOR PROTEIN-2 μ -adaplin by ADAPTOR-ASSOCIATED KINASE1 regulates root tropic growth

Wei Siao,^{1,2} Peng Wang,^{1,2} Xiuyang Zhao,^{1,2} Lam Dai Vu,^{1,2} Ive De Smet,^{1,2} and Eugenia Russinova,^{1,2,*,\ddagger}

¹ Department of Plant Biotechnology and Bioinformatics, Ghent University, 9052 Ghent, Belgium

² Center for Plant Systems Biology, VIB, 9052 Ghent, Belgium

*Author for correspondence: eurus@psb.ugent.be

\ddaggerSenior author

The author responsible for distribution of materials integral to the findings presented in this article in accordance with the policy described in the instructions for Authors (<https://academic.oup.com/plcell/pages/General-Instructions>) is: Eugenia Russinova (eurus@psb.vib-ugent.be).

ABSTRACT

ADAPTOR-ASSOCIATED PROTEIN KINASE1 (AAK1) is a known regulator of clathrin-mediated endocytosis in mammals. Human AAK1 phosphorylates the μ 2 subunit of the ADAPTOR PROTEIN-2 (AP-2) complex and plays an important role in cell differentiation and development. Previous interactome studies had discovered the association of AAK1 with AP-2 in Arabidopsis, but its function remained unknown. Here, genetic analysis revealed that the Arabidopsis *aak1* and *ap2m* mutants both displayed an altered root tropic growth, including impaired touch- and gravity-sensing responses. In Arabidopsis, AAK1 phosphorylated AP2M on Thr-163, and expression of AP2M phospho-null version into the *ap2m* mutant led to an *aak1*-like phenotype, whereas the phospho-mimic forms of AP2M rescued the *aak1* mutant. In addition, we found that AAK1-dependent phosphorylation state of AP2M modulates the frequency distribution of endocytosis. Our data indicate that the AP2M phosphorylation on Thr-163 by AAK1 fine-tunes endocytosis in the Arabidopsis root to control its tropic growth.

INTRODUCTION

The dynamic turnover of plasma membrane (PM) proteins is tightly regulated by the rates of endocytosis, degradation, and protein delivery to the PM via secretion or recycling. The best-characterized route for PM protein internalization is the clathrin-mediated endocytosis (CME) through clathrin-coated vesicles (CCVs) (Traub, 2009; McMahon and Boucrot, 2011). In mammalian cells, CCVs develop from clathrin-coated pits (CCPs) that are formed by the assembly of the major coat proteins, clathrin and the ADAPTOR PROTEIN-2 (AP-2) (Roth and Porter 1964; Kirchhausen et al., 2014). Low amounts of other clathrin adaptors and CME accessory proteins are also found in CCVs that function as scaffolds, cargo recruiters, membrane curvature generators, and CME regulators (Borner et al., 2012; Mettlen et al., 2018).

The mammalian heterotetrameric AP-2 complex consists of two large subunits (α 2 and β 2), one medium subunit (μ 2), and one small subunit (σ 2). By binding to phosphatidylinositol 4,5-bisphosphate (PIP₂), the inactive, closed form of cytosolic AP-2 is initially recruited to the PM, where AP-2 is conformationally changed to an active, open form that is favored by phosphorylation on Thr-156 in the μ 2 subunit (Collins et al., 2002; Höning et al., 2005). Previous data suggest that phosphorylation of the human μ 2 enhances binding to phospholipids and cargoes (Ricotta et al., 2002; Höning et al., 2005) and that mutation in the phosphorylation site inhibits transferrin uptake (Olusanya et al., 2001). However, later studies have shown that, although μ 2 Thr-156 phosphorylation stabilizes the open AP-2 form, unphosphorylated AP-2 can readily bind to cargo-containing membranes and the cargo affinity is not enhanced by the

Thr-156 phosphorylation of the $\mu 2$ (Jackson et al., 2010; Kelly et al., 2014; Kadlecova et al., 2016; Wrobel et al., 2019).

A NUMB-ASSOCIATED KINASE (NAK) family member, ADAPTOR-ASSOCIATED KINASE1 (AAK1), phosphorylated $\mu 2$ *in vitro* and co-purified with AP-2 in CCVs in human cells (Conner and Schmid, 2002; Ricotta et al., 2002; Borner et al., 2012; Sorrell et al., 2016). However, gene silencing of *AAK1* did not alter the AP-2 phosphorylation status in cells and the AAK1-phosphorylated Thr-156 in $\mu 2$ negatively regulated the AP2-dependent transferrin endocytosis (Conner and Schmid, 2002; Conner and Schmid, 2003; Henderson and Conner, 2007; Partlow et al., 2019). Through regulating CME, the human AAK1 was found to regulate negatively and positively the β -catenin-dependent WNT (Agajanian et al., 2019) and the Notch (Gupta-Rossi et al., 2011) signaling pathways, respectively. Silencing of *AAK1* also interfered with some AP2-independent events, such as accumulation of transferrin receptors in perinuclear endosomes, reduced viral entry of vesicular stomatitis virus, and inhibition of LOW DENSITY LIPOPROTEIN (LDL) uptake (Pelkmans et al., 2005; Henderson and Conner, 2007). Hence, human AAK1 plays multiple roles in different pathways.

Recently, a crystal structure study identified an open and active conformation of AP-2, designated open+, of which the “bowl” (α trunk, $\beta 2$ trunk, $\mu 2$ N-terminus, and $\sigma 2$) superimposed well with that of the open form (Wrobel et al., 2019). The main difference between the open and the open+ conformers is the different orientation of the $\mu 2$ C-terminus (Wrobel et al., 2019). In the current mammalian model, unphosphorylated AP-2 is already in equilibrium between the open and open+ forms on the PM, with the open+ form only compatible with the Thr-156 phosphorylation in $\mu 2$ (Kelly et al., 2014; Wrobel et al., 2019). Therefore, the Thr-156 phosphorylation in $\mu 2$ affects the CCP maturation and the CME rate, because of the stabilizing ability of the open+ cargo-binding conformation of AP-2, but not of alterations in the efficiency of cargo sequestration (Wrobel et al., 2019).

In Arabidopsis the AP-2, which consists of two large subunits (AP2A and AP2B), one medium subunit (AP2M) and one small subunit (AP2S), similarly facilitates CME of various PM proteins (Di Rubbo et al., 2013; Kim et al., 2013; Yoshinari et al., 2019; Liu et al., 2020). In contrast to the embryo lethal phenotype of a single *ap2* subunit knockout in mice (Mitsunari et al., 2005), in Arabidopsis mutants in single subunits of AP-2 display relatively mild growth phenotypes, such as slender rosette leaves, short petioles, defects in staminal filament and pollen tube elongation, and reduced fertility (Di Rubbo et al., 2013; Fan et al., 2013; Kim et al., 2013; Yamaoka et al., 2013). A recent interactome study has identified the Arabidopsis AAK1

as a binding partner of AP-2 in Arabidopsis (Wang et al., 2023), but the function of AAK1 remained unelucidated as well as the phospho-regulation of AP2M.

Here, we show that the Arabidopsis AAK1 is an active serine/threonine kinase that can phosphorylate AP2M on Thr-163 *in vitro*. A knockout of the *AAK1* altered the root tropic growth due to decreased waving, reduced gravitropic bending, and enhanced obstacle avoidance, whereas knockout of *AP2M* resulted in previously unreported and contrasting root behavior, namely increased waving, skewing, agravitropism, and root curling when impenetrable surfaces were encountered. By means of genetic studies we reveal that the phosphorylation of AP2M on Thr-163 *in planta* determines the root behavior. We also demonstrate that AAK1 maintains the balance of endocytosis in root cells and fine-tunes the AP2M function through phosphorylation.

RESULTS

Arabidopsis AAK1 is an active kinase and phosphorylates AP2M on Thr-163 *in vitro*

Previously, by means of an interactome study we had identified a protein kinase superfamily protein (AT2G32850) that copurified specifically with AP-2 and was orthologous to the mammalian AAK1 (Wang et al., 2023). Phylogenetic analysis across eukaryotic species indicated that contrary to the mammalian *AAK1* gene, which belongs to the highly diverse NAK family (Sorrell et al., 2016) and other plant species, such as maize (*Zea mays*) and rice (*Oryza sativa*), with duplicate genes, the Arabidopsis *AAK1* is a single-copy gene (Supplemental Figure S1A). Similar to the human AAK1 (Conner and Schmid, 2002), the Arabidopsis AAK1 contains an N-terminal kinase domain and two adaptin-binding motifs (WXXFXD and WXXF) in the C-terminus (Figure 1A), but in contrast, the QP-rich middle domain is replaced by a coiled-coil domain (Figure 1A; Supplemental Figure S1B). The kinase domain of Arabidopsis AAK1 is 43% identical and 62% similar that of the human AAK1 and the catalytic sites are well conserved (Supplemental Figure S1C). The protein domain structure and the association with AP-2 (Wang et al., 2023) altogether suggest that the Arabidopsis AAK1 might also function as an AP-2 kinase.

To test whether the Arabidopsis AAK1 is an active kinase, we generated maltose-binding protein (MBP)-tagged recombinant proteins of the wild type AAK1 (MBP-AAK1) and two putative AAK1 kinase-dead versions (MBP-AAK1^{K57A} and MBP-AAK1^{D157A}) by mutating the conserved residues within the kinase domain (Conner and Schmid, 2003) (Figure 1A; Supplemental Figure S1C). An *in vitro* kinase assay revealed that the wild type AAK1 exhibited

autophosphorylation activity, whereas the two kinase-dead versions of AAK1 did not (Figure 1B), implying that AAK1 is an active kinase.

The human AAK1 phosphorylates the $\mu 2$ subunit of AP-2 at a single Thr-156 residue (Ricotta et al., 2002) that is conserved with the Thr-163 in the Arabidopsis AP2M (Figure 1C). Searches in the Plant PTM Viewer (<https://www.psb.ugent.be/webtools/ptm-viewer>) (Vu et al., 2016; Willems et al., 2019) and PhosPhAt (<https://phosphat.uni-hohenheim.de/db.html>) (Zulawski et al., 2013) databases indicated the occurrence of three AP2M phosphorylated residues *in planta* (Thr-163, Thr-159, and Ser-144) (Mergner et al., 2020) (Supplemental Figure S2A). To determine whether the Arabidopsis AAK1 can phosphorylate AP2M, we carried out an *in vitro* kinase assay with bacterially produced glutathione S-transferase (GST)-tagged AP2M and the MBP-tagged AAK1, but did not detect phosphorylation on GST-AP2M (Supplemental Figure S2B), probably because the recombinant AP2M protein either did not fold properly or the phosphorylation residue was inaccessible to AAK1.

By means of a short synthetic peptide fused with a GST tag containing Thr-159 and Thr-163 residues (GST-AP2M-T163) we tested whether AAK1 phosphorylates the Thr-163 residue in AP2M. The *in vitro* kinase assay demonstrated that the short peptide was phosphorylated, whereas the GST fusion protein bearing a mutated peptide in which only the Thr-163 had been substituted with alanine (GST-AP2M-T163A) was not (Figure 1D). However, phosphorylation on Thr-163 in the GST-AP2M-T163 peptide was not identified by mass spectrometry (MS) (Supplemental Dataset 1), likely because of technical limitations. Altogether, our data demonstrate that AAK1 phosphorylates AP2M on Thr-163 but not Thr-159 *in vitro*.

AAK1 regulates root waving and gravitropism in Arabidopsis

We next assessed the function of AAK1 in Arabidopsis. *pAAK1:nlsGFP* reporter revealed that *AAK1* is ubiquitously expressed (Supplemental Figure S3, A-C). Subsequently, we identified one T-DNA insertion mutant (SALK_001684) (Figure 2A) and generated transgenic plants overproducing the kinase by transforming the wild type Arabidopsis with the *AAK1* genomic DNA driven by the cauliflower mosaic virus (*CaMV*) 35S promoter. Immunoblot analysis with a specific α -AAK1 antibody revealed that the SALK_001684 allele, hereafter designated *aak1-1*, was a knockout mutant and the overexpression (OE) line, hereafter designated AAK1OE, had accumulated more AAK1 protein than did the wild type accession, Columbia-0 (Col-0) (Figure 2B). Neither the *aak1-1* mutant nor the AAK1OE plants displayed any obvious growth defects throughout the vegetative and reproductive stages (Supplemental Figure S4, A and B). Interestingly, 5-day-old *aak1-1* and AAK1OE seedlings had slightly less and more wavy

primary roots than the wild type, respectively whereas the primary root length of the two genotypes was similar to that of the wild type (Figure 2, C-E). To confirm that the differences in root behavior resulted from the AAK1 dysfunction, we deleted the *AAK1* gene by CRISPR/Cas9 technology from the 45th to the 2359th bp, hereafter referred to as the *aak1-2* mutant (Figure 2A). In addition to *aak1-2*, we also identified *aak1-3* that had one nucleotide inserted 44 bp after the start codon, with a premature termination codon after the 29th amino acid as a consequence (Figure 2A). No AAK1 protein was detected in *aak1-2* and *aak1-3* by immunoblotting with an α -AAK1 (Figure 2B), indicating that the two mutants were also knockout mutants. Identical to *aak1-1*, both the primary roots of 5-day-old *aak1-2* and *aak1-3* seedlings were less wavy than those of the wild type (Figure 2, C and E), whereas leaves and siliques developed normally (Supplemental Figure S4, A and B). In addition to root waving, the early gravitropic responses were compromised in the *aak1* mutants (Figure 2F; Supplemental Figure S4C) thus, hinting at impaired auxin transport. In agreement, the polarity of PIN2-GFP was moderately altered in *aak1-1* root meristem (Supplemental Figure S4, D and E).

To corroborate that the observed root phenotypes were caused by a mutation in the *AAK1* gene, we complemented the *aak1-1* mutant with a construct containing the genomic *AAK1* DNA fused at the 3' end to the green fluorescent protein (GFP) gene under the control of the native *AAK1* promoter. Two independent homozygous transgenic lines, *pAAK1:AAK1-GFP/aak1-1* (lines #1 and #4) were characterized (Figure 2B). Expression of AAK1-GFP in *aak1-1* restored the root waving and gravitropic bending back to the wild type (Figure 2, C-F), suggesting that the *pAAK1:AAK1-GFP* construct is functional.

Subsequently, we examined the subcellular localization of AAK1-GFP in *pAAK1:AAK1-GFP/aak1-1* line #1 and detected that AAK1-GFP was mainly located in the cytoplasm. Although some punctate-like structures were observed (Supplemental Figure S3, D-F), the structures are either transvacuolar strands or uneven distribution in the cytoplasm (Supplemental Movie 1). Whether trace amounts of AAK1-GFP localized on the endosome was examined by the simultaneous staining of the root cells with FM4-64 and treatment with brefeldin A (BFA). After 30 min of treatment, AAK1-GFP remained cytoplasmic without aggregation (Supplemental Figure S3G), indicating that AAK1-GFP did not localize to the *trans*-Golgi network/early endosome. Time-lapse imaging of the PM (Supplemental Figure S3H) revealed lack of punctate signals, indicating that AAK1 functions in the cytoplasm. In summary, AAK1 is ubiquitously expressed cytoplasmic kinase that controls primary root waving and gravity sensing during seedling stage.

AP2M functions downstream of AAK1

Given that the Arabidopsis AAK1 phosphorylated AP2M *in vitro*, we hypothesized that AAK1 regulates the AP-2 function and, hence, that the root behavior of the *ap2m* mutant might also be affected. Although the *ap2m* mutant displayed a number of growth-related phenotypes (Kim et al., 2013; Yamaoka et al., 2013), no root phenotypes have been previously described. Interestingly, in contrast to the *aak1* mutants, the primary root of the 5-day-old *ap2m-2* mutant exhibited enhanced waving and skewing and was longer than that of the wild type (Figure 2, C-E). To verify that these root phenotypes were due to the *AP2M* mutation, we generated an additional *ap2m* mutant by CRISPR/Cas9 technology. The obtained CRISPR mutant of *AP2M*, hereafter designated *ap2m-3*, had a single nucleotide deleted 76 bp after the start codon, resulting in a premature stop codon after the 28th amino acid (Supplemental Figure S4F). In addition to the previously reported growth phenotypes (Kim et al., 2013; Yamaoka et al., 2013), *ap2m-3* showed the same primary root phenotypes as *ap2m-2* (Figure 2, C-E; Supplemental Figure S4, A and B). The root gravitropic assay also revealed that the root bending angles of *ap2m-2* and *ap2m-3* were deviated from the gravity vector (Figure 2F; Supplemental Figure S4C). Thus, AP2M regulates not only growth and development of leaves and reproductive organs, but also the root behavior.

As the root phenotypes pertaining to root waving differed in the *aak1* and *ap2m* mutants, we generated the *aak1-1 ap2m-2* double mutant and found that it exhibited root phenotypes similar to the *ap2m-2* including a longer primary root, an enhanced root waving and skewing behavior, a disrupted root gravitropic bending, slender rosette leaves, shortened petioles, and reduced silique size (Figure 2, C-E; Supplemental Figure S4, A and B). Hence, *AP2M* was epistatic to *AAK1* and might be a downstream target. In addition, we also examined the root phenotype of the *pAP2M:AP2M-GFP/ap2m-2* complemented line, which could rescue the leaf, flower and silique phenotypes of *ap2m-2* (Yamaoka et al., 2013). Intriguingly, although the expression of AP2M-GFP in *ap2m-2* could rescue the leaf and silique phenotypes (Supplemental Figure S4, A and B) (Yamaoka et al., 2013), the roots of the *pAP2M:AP2M-GFP/ap2m-2* plants were similar to those of the *aak1* mutant and were less wavy (Figure 2, C-E), indicating that the C-terminally positioned GFP somehow modifies the function of AP2M in the root. In agreement, co-immunoprecipitation (Co-IP) analysis with *pAP2M:AP2M-GFP/ap2m-2* and *pAP2S:AP2S-GFP/ap2s* transgenic Arabidopsis revealed that the endogenous AAK1 co-purified with AP2S-GFP, but not with AP2M-GFP (Figure 4C). Hence, the GFP tag

disabled AAK1 to interact with AP2M-GFP and is possibly the reason for the roots of *pAP2M:AP2M-GFP/ap2m-2* to behave like those of the *aak1* mutants.

AAK1 and AP2M regulate root touch responses

Since root waving is a combined response to gravity and mechanical stimuli (Oliva and Dunand, 2007), we investigated the root touch response and medium penetration ability of *aak1* and *ap2m* mutants by growing the seedlings horizontally on medium containing different concentrations of agar (0.4%, 0.6%, 1%, and 1.2%). When grown horizontally on medium supplemented with 0.4% agar, approximately half of the wild type roots penetrated the medium, whereas the root penetration of *aak1-1*, *aak1-2*, *aak1-3*, AAK1OE, and *ap2m-2* was reduced and that of the *pAAK1:AAK1-GFP/aak1-1* plants slightly increased (Supplemental Figure S5A). The root penetration of all genotypes was dramatically reduced when grown in 0.6% agar (Supplemental Figure S5B) and almost none of the genotypes could penetrate 1% or 1.2% agar medium (Figure 3, A and B; Supplemental Figure S5C). When the roots were unable to penetrate the 1% and 1.2% agar medium, three different root growth behaviors were observed: (i) root, growing continuously toward the gravity vector and causing detachment from the medium and formation of an arch shape, defined as “arch root” and occurring mostly in the wild type Col-0 (Figure 3A; Supplemental Figure S5D); (ii) root, growing wavyly along the surface of the agar medium, typical of the *aak1* mutants, defined as “wavy root” (Figure 3A and Supplemental Figure S5E); and (iii) root, growing along the surface of the agar with spiral curls, distinctive of the *ap2m-2* mutant, defined as “curly root” (Figure 3A; Supplemental Figure S5F). As roots had less chance to penetrate 1.2% agar than 1% agar, we performed the root horizontal growing assay on 1.2% agar medium with reproducible results (Figure 3, A and B).

When grown on 1.2% agar medium, about 88% of the Col-0 roots were of the arch type and approximately 10% of the wavy root type (Figure 3B). The roots of the *aak1-1*, *aak1-2*, and *aak1-3* mutants exhibited approximately 72% wavy, 24% arch, and 4% curly root types. The roots of *ap2m-2* and *aak1-1 ap2m-2* both displayed approximately 77% curly, 12% wavy, and 11% arch root types. Introduction of *pAAK1:AAK1-GFP* into *aak1-1* rescued the root behavior back to the wild type, whereas the roots of AAK1OE displayed a root behavior mixed between Col-0 and *aak1*, with 64% arch and 34% wavy root types (Figure 3B). The above data indicate that AAK1 and AP2M play roles in the behavior of roots growing on an impenetrable surface, probably by modulating the gravitropic and touch responses.

Arabidopsis AAK1 regulates the root behavior by phosphorylating AP2M on Thr-163

To assess the physiological function of AP2M phosphorylation, we introduced the phospho-null version of AP2M (AP2M^{T163A}) into the *ap2m* mutant. As *pAP2M:AP2M-GFP/ap2m-2* exhibited an *aak1*-like root phenotype in both the vertical (Figure 2, C-E) and horizontal assays (Figure 4, A and B), we inserted a tag-free version of AP2M into the *ap2m-3* mutant. The root horizontal assay revealed that *ap2m-3* displayed the same curly root type behavior as *ap2m-2* (Figure 4, A and B). Introduction of the wild type genomic DNA of *AP2M*, including the promoter region (*pAP2M:AP2M*), into the *ap2m-3* mutant not only rescued the leaf and silique phenotype (Supplemental Figure S4, G and H), but also reversed the curly root type back to arch root type as in the wild type (Figure 4, A and B), indicating that the tag-free version of AP2M fully rescued the *ap2m* phenotype. By contrast, even though the introduced phospho-null version of AP2M (*pAP2M:AP2M^{T163A}*) rescued the leaf and silique phenotype (Supplemental Figure S4, G and H), the root behavior of *pAP2M:AP2M^{T163A}/ap2m-3* resembled that of the *aak1* mutants, of which the roots bent and grew along the agar surface (Figure 4, A and B), implying that the phosphorylation state of AP2M plays a critical role in controlling the root behavior, which can be a combined result of the crosstalk between root gravitropic and touch responses.

We next tested whether the kinase activity of AAK1 is required for the root behavior on hard agar surfaces, we introduced the kinase-dead versions of AAK1 under the control of the endogenous promoter (*pAAK1:AAK1^{K57A}* and *pAAK1:AAK1^{D157A}*) into *aak1-1* and analyzed the root phenotypes of three homozygous lines for each kinase-dead construct. As expected, none of the AAK1 kinase-dead versions rescued the root behavior of *aak1-1* (Supplemental Figure S6, A and B) concluding that the kinase activity of AAK1 is essential for its physiological function *in planta*.

To demonstrate the importance of Thr-163 phosphorylation in AP2M, we introduced two phospho-mimic forms of AP2M (*pAP2M:AP2M^{T163D}* and *pAP2M:AP2M^{T163E}*) and a phospho-null form of AP2M (*pAP2M:AP2M^{T163A}*) into the *aak1-1* mutant. By screening 12 independent T2 heterozygous lines for each construct by the root horizontal assay, we found that 10 out of 12 lines of *pAP2M:AP2M^{T163E}/aak1-1* and 7 out of 12 lines of *pAP2M:AP2M^{T163D}/aak1-1* complemented the *aak1* (Supplemental Figure S7A). In contrast, the 12 *pAP2M:AP2M^{T163A}/aak1-1* lines still had a wavy root behavior (Supplemental Figure S7A). Two independent transgenic lines for each construct, *pAP2M:AP2M^{T163A}/aak1-1* (lines #1 and #2), *pAP2M:AP2M^{T163D}/aak1-1* (lines #1 and #2) and *pAP2M:AP2M^{T163E}/aak1-1* (lines #1 and #2) were further analyzed (Figure 4, D and E). The results showed that the roots of

pAP2M:AP2MT^{163D}/aak1-1 and *pAP2M:AP2MT^{163E}/aak1-1* behaved like the wild type, but those of the *pAP2M:AP2MT^{163A}/aak1-1* lines still like the *aak1* mutants (Figure 4, D and E), indicating that the phospho-mimic forms of AP2M rescued the *aak1-1* phenotype, whereas the phospho-null form of AP2M did not. Quantitative reverse transcription PCR (RT-qPCR) analysis of *AP2M* transcripts in the transgenic lines (*AP2M*, *AP2M^{T163A}*, *AP2M^{T163D}* and *AP2M^{T163D}*) in different background (*ap2m-3* and *aak1-1*) confirmed that the root behavior was associated with the mutated AP2M versions not the *AP2M* expression levels (Supplemental Figure S7B).

In summary, the Arabidopsis AAK1 regulates the root behavior in response to impenetrable surfaces through AP2M phosphorylation on Thr-163.

Phosphorylation of AP2M on Thr-163 by AAK1 regulates the endocytosis rates

Mutation of the phosphorylated threonine (T156A) in the human μ 2 subunit has been shown to inhibit transferrin uptake in tissue cultures (Olusanya et al., 2001). Therefore, we examined whether endocytosis is affected in the *aak1* mutants and the transgenic Arabidopsis expressing phospho-null mutation of AP2M in *ap2m-3* background by means of FM4-64 uptake. Unexpectedly, unlike the *ap2m-2* and *ap2m-3* mutants that exhibited an obviously reduced FM4-64 uptake in the root epidermal cells, the FM4-64 uptake was not reduced in *aak1-1*, *aak1-2*, and *pAP2M:AP2M^{T163A}/ap2m-3* (Figure 5, A and B), but rather was slightly higher than that of the wild type. The FM4-64 uptake did not significantly differ between the wild type and AAK1OE and the introduction of *pAP2M:AP2M* into *ap2m-3* rescued the FM4-64 uptake to the wild type level (Figure 5, A and B), indicating that the unphosphorylated AP2M is still functional in Arabidopsis and AAK1 is likely required to tune down endocytosis.

In addition, we noticed that, although most of the FM4-64 internalization events were similar between the wild type and the *aak1* mutants, a small population of cells showed an elevated FM4-64 uptake (Figure 5B). Therefore, a more detailed analysis on the population distributions was carried out. First, by a normality test, we found that the FM4-64 uptake of most genotypes, except *ap2m-2*, were not normally distributed (Supplemental Figure S8), suggesting that judging the FM4-64 uptake rates by means of the average (arithmetic mean) values might not be fully representative. Therefore, we plotted the relative frequency distribution histograms and found that the FM4-64 uptake distribution of *aak1-1*, *aak1-2*, and *pAP2M:AP2M^{T163A}/ap2m-3* were flatter and wider than those of the others (Figure 5C). Nonlinear curve fitting showed that the FM4-64 uptake distribution of the wild type had two peaks, a major and a minor one centered at 0.36 and at 0.58, respectively, and that the results

of the *pAP2M:AP2M/ap2m-3* complementation line were similar, namely with a major and minor peak at 0.39 and at 0.61, respectively (Figure 5C), but the fitted curves of *ap2m-2* and *ap2m-3* were more symmetric and had single peaks at 0.29 and 0.28, respectively (Figure 5C). Interestingly, the distributions of *aak1-1*, *aak1-2*, and *pAP2M:AP2M^{T163A}/ap2m-3* were multimodal with three peaks: *aak1-1* had two major and one minor peaks centered at 0.37 and 0.52 and at 0.71, respectively; *aak1-2* had two major and one peaks at 0.37 and 0.54 and at 0.76, respectively; and *pAP2M:AP2M^{T163A}/ap2m-3* had two major and one minor peaks at 0.38 and 0.53 and at 0.71, respectively (Figure 5C). The extra minor peaks with higher ratios of FM4-64 internalization were the reason for the significantly higher average values than those of the wild type, only when the sample size was large enough. By contrast, the distribution of AAK1OE was lognormal with one geometric mean at 0.38, indicating that, albeit no significant differences on the averages by the Kruskal-Wallis test (Figure 5B), the endocytosis was weakly affected in the AAK1OE cells.

To examine whether CME of different PM cargos is affected by the absence of AAK1 first, we investigated the internalization of the fluorescent brassinosteroid (BR) analog, Alexa Fluor 647-castasterone (AFCS), which is a ligand of the BR-INSENSITIVE1 (BRI1) receptor (Irani et al., 2012; Di Rubbo et al., 2013), in root cells of *aak1-1* mutant. Comparable to the FM4-64 uptake, AFCS internalization was slightly higher in *aak1-1* than that of Col-0 (Figure 6, A and B). The frequency distribution of the AFCS endocytosis in Col-0 was more centered than that in *aak1-1*, which had a higher deviation (Figure 6C). Similarly, the cytoplasmic versus PM fluorescence intensity ratio of another CME cargo, PIN2-GFP (Kitakura et al., 2011; Adamowski et al., 2018) was slightly higher in root cells of *aak1-1* than that of the wild type (Figure 6, D-F). In addition, the accumulation of PIN2-GFP in Brefeldin A (BFA)-induced compartments (so-called BFA bodies) in *aak1-1* was increased compared to the wild type (Figure 6, G and H). However, no significant differences in BFA body dissipation after the BFA washout were observed between the wild type and the *aak1-1* mutant (Figure 6, G and I), implying that AAK1 regulates PIN2 endocytosis, but not recycling to possibly control its polar localization in the Arabidopsis root meristem (Supplemental Figure S4, D and E).

Taken together, we conclude that Arabidopsis AAK1 controls the CME homeostasis of different PM cargoes in the root and thus it affects its gravitropic and touch responses

DISCUSSION

In mammalian cells, the AP-2 complex is essential for CCV formation, and the null *ap2m* mutant in mice is embryonic lethal (Collins et al., 2002; Mitsunari et al., 2005). In Arabidopsis, although the AP-2 is required for efficient CME, the *ap2m* and *ap2s* mutants are viable, albeit defects in leaf morphology, staminal filament elongation, pollen tube growth, and the silique development (Fan et al., 2013; Kim et al., 2013; Yamaoka et al., 2013). Nonetheless, the function of AP-2 in root growth and development has not been assessed yet. Here, we report that the primary root of the *ap2m* null mutant grew faster than the wild type, but displayed agravitropic, wavy, and skewing phenotypes during the seedling stage. When grown on impenetrable horizontal plates, the primary root of the *ap2m* mutant had a curly root behavior, distinctive from that of the wild type. These root phenotypes are probably due to defective endocytosis in the root cells, disturbing the auxin polar transport (Dhonukshe et al., 2007; Men et al., 2008; Kitakura et al., 2011).

Our previous AP interactome studies had discovered an association between AP-2 and an unknown kinase that is similar to the mammalian AAK1 (Wang et al., 2023). The roles of the mammalian AAK1 in phosphorylating the $\mu 2$ subunit of AP-2 on a threonine residue (Thr-156) and in regulating the AP-2 activity have been widely reported, but also debated (Olusanya et al., 2001; Conner and Schmid, 2002; Ricotta et al., 2002; Höning et al., 2005; Partlow et al., 2019; Wrobel et al., 2019). Although several lines of evidence suggest that the Thr-156 phosphorylation in $\mu 2$ is required for cargo recognition via a phosphorylation-activated conformational change promoting cargo and membrane binding (Olusanya et al., 2001; Collins et al., 2002; Ricotta et al., 2002; Höning et al., 2005), this hypothesis somehow conflicts with the temporal ordering of CCV formation, because AP-2 should have bound to the PM and the cargo before its phosphorylation by AAK1 (Wrobel et al., 2019). Besides, AP-2 has been shown to bind to PtdIns(4,5)P₂- and cargo-containing membranes without being phosphorylated and the Thr-156 phosphorylation of $\mu 2$ not to have a major effect on the cargo affinity of AP-2 (Jackson et al., 2010; Kelly et al., 2014; Kadlecova et al., 2016; Wrobel et al., 2019). Instead, $\mu 2$ phosphorylation increases its affinity to ADAPTIN EAR-BINDING COAT-ASSOCIATED PROTEINS (NECAPs) and is the key determinant in timing and recruitment of NECAP-1 in the AP-2 regulatory cycle and, thus, modulate CCV formation and CME (Partlow et al., 2019; Wrobel et al., 2019). The AP interactome in Arabidopsis also identified a putative NECAP-1 homolog that interacts with AP-1 and AP-2 subunits (Wang et al., 2023). In mammalian systems, the newly identified active open+ conformation of AP-2 and the co-regulation with NECAPs might explain some of the discrepancies (Kelly et al., 2014; Wrobel et al., 2019), although whether NECAPs play a positive or inhibitory role in the AP-2 activation remains a

matter of debate (Beacham et al., 2018; Partlow et al., 2019; Wrobel et al., 2019). Additionally, AAK1 could function redundantly with the NAK family kinases, such as the cyclin G-associated kinase (GAK) (Umeda et al., 2000) and the bone morphogenic protein (BMP)-inducible kinase (BIKE) (Sorrell et al., 2016), or has other functions (Conner and Schmid, 2003; Henderson and Conner, 2007). Interestingly, mammalian AAK1 is activated by clathrin (Conner et al., 2003), however, clathrin binds the already opened AP-2 form in the PM (Kelly et al., 2014). Currently, the mechanism of AAK1 activation is unclear. It has been suggested that the substrate binding site of AAK1 may be blocked by its C-terminal region that can be removed through clathrin binding (Jackson et al., 2003), but later evidence showed that clathrin can also activate the C-terminally truncated AAK1 (Conner et al., 2003). It has also been speculated that phosphorylation may regulate AAK1 activity, since there are several phosphorylation sites in the kinase domain of human AAK1 (Sorrell et al., 2016) and one site in that of Arabidopsis AAK1 (Supplemental Figure S1C) (Mergner et al., 2020). However, the activity of human AAK1 is not dependent on phosphorylation (Sorrell et al., 2016).

In human cells AAK1 seemingly inhibits AP-2-dependent transferrin internalization, both *in vitro* and *in vivo* (Conner and Schmid, 2002; Conner and Schmid, 2003) and μ 2 phosphorylation might function in an inactivation process (Partlow et al., 2019). Silencing of *AAK1* did not induce changes in AP2M phosphorylation, transferrin uptake, or AP-2 distribution (Conner and Schmid, 2003; Henderson and Conner, 2007). By means of amphiphilic styryl dyes, such as FM4-64, that particularly imbed in the outer membranes with a specific phospholipid composition in both mammalian and plant cells (Richards et al., 2000; Van Gisbergen et al., 2008; Dason et al., 2010), distinct vesicle pools of endocytic routes can be labeled. In neurons, FM4-64 is sequestered into synaptic vesicles (Newton and Murthy, 2006; Chen et al., 2008), whereas in plant cells, FM4-64 is taken up by CME, flotillin-mediated endocytosis, and bulk-flow endocytosis (Bolte et al., 2004; Baral et al., 2015). Our data showed that the FM4-64 uptake in *aak1* mutants is increased and the frequency distribution flatter than those of the wild type. A similar trend was observed for two other plant CME cargoes, AFCS and PIN2-GFP. AFCS is a fluorescent BR analog that is internalized together with the BRI1 receptor (Irani et al., 2012), whereas PIN2 is an auxin efflux carrier that mediates auxin gradients in the Arabidopsis root by its polar PM localization in cortex and epidermal cells and thus, directs root gravitropism. The establishment and maintenance of PIN2 polarity is controlled by CME (Kitakura et al., 2011; Adamowski et al., 2018). Conversely, although the average value of FM4-64 uptake in plants overproducing AAK1 was the same as that of wild type, the FM4-64 uptake distribution in these plants was slightly skewed to the left. Hence,

Arabidopsis AAK1 might regulate the endocytic homeostasis and play an inhibitory role in endocytosis, consistent with finding in mammals (Conner and Schmid, 2002; Conner and Schmid 2003; Partlow et al., 2019).

Our phylogenetic analysis revealed that the Arabidopsis AAK1 is a single-copy gene and that no other kinase homolog is present in the Arabidopsis genome. The Arabidopsis *AAK1* knockout mutant displays less root waving and a reduced gravitropic response on vertical plates, but an increased obstacle avoidance response on horizontal plates. In addition, introduction of the kinase-dead versions of AAK1 in *aak1-1* fails to rescue the *aak1* phenotype, which successfully rescued by the phospho-mimic, but not the phospho-null, forms of AP2M, suggesting that AAK1 may be the only kinase that phosphorylates AP2M at Thr-163 in Arabidopsis. Furthermore, expression of the phospho-null form of AP2M in the *ap2m-3* mutant resulted in an *aak1*-like behavior. The *aak1* and *ap2m* mutants also exhibit opposite root phenotypes when grown on vertical plates. Altogether these data imply that AAK1 may negatively regulate the AP-2 activity by phosphorylating AP2M on Thr-163. Next, by an *in vitro* kinase assay using isotope labeling, we demonstrated that Arabidopsis AAK1 can phosphorylate the Thr-163 residue in AP2M. However, this phosphorylation event was not identified by our MS analysis despite that it was previously detected *in planta*.

The plant root behavior is complex, because it is the sum of the output of the root tropic responses (e.g., gravitropism, thigmotropism, hydrotropism, and halotropism) and of autonomous movement (such as, circumnutation) (Eapen et al., 2005; Brooks et al., 2010; Galvan-Ampudia et al., 2013; Jacobsen et al., 2021; Loshchilov et al., 2021). PIN-FORMED (PIN)-mediated polar auxin transport and ethylene signaling have been shown to regulate root gravitropism and mechanical responses (Růzicka et al., 2007; Yamamoto et al., 2008; Zhang and Friml, 2020; Jacobsen et al., 2021), whereas abscisic acid and BRs play major roles in root hydrotropism (Eapen et al., 2005; Dietrich et al., 2017; Miao et al., 2018). The root behaviors of the *aak1* and *ap2m* mutants in the vertical and horizontal assays are probably due to the altered gravitropism and touch responses, because the root gravitropic bending is affected in the mutants and the main factors in the assays are the agar concentration and the plate orientations. A similar root horizontal assay and root behaviors have been reported, but not used to identify mutants (Tojo et al., 2021). Nonetheless, we cannot exclude that hydrotropism and drought avoidance might also contribute to the root behaviors, because the water potential of the medium decreases linearly with increasing agar concentrations (Ghashghaie et al., 1991).

As endocytosis is essential for many cellular functions and signaling cascades, changes in the balance between endocytosis and other vesicle trafficking may disturb the dynamics of

receptors and transporters on the PM, in turn, affecting the hormone signaling pathways (Dhonukshe et al., 2007; Kitakura et al., 2011; Di Rubbo et al., 2013; Xia et al., 2019; Liu et al., 2020) with modified root tropic responses and behaviors as a consequence. In the wild type, when the Thr-163 of AP2M is phosphorylated by AAK1, endocytosis is regulated, and the roots exhibit normal gravitropic responses when grown vertically on the agar surface and pointed toward the gravitropic vector even when encountering the impenetrable medium. In the absence of AP2M the endocytosis rates in the root cells are reduced, resulting in agravitropic and curly roots on vertical and horizontal plates, respectively. When only unphosphorylated AP2M is present in the cells, e.g., in the *aak1* null mutants, *AP2M-GFP/ap2m-2*, and *AP2M^{T163A}/ap2m-3*, the balance and endocytosis coordination in the root cells are affected, leading to a reduced root gravitropic bending and an enhanced obstacle avoidance response on vertical and horizontal plates, respectively.

In summary, we revealed the regulatory mechanisms of the AP-2 accessory protein, AAK1, on AP2M phosphorylation in Arabidopsis, i.e., the Arabidopsis AAK1 phosphorylates AP2M on Thr-163 and the phosphorylation maintains the endocytosis balance in root cells and controls the root behaviors. Our findings suggest that AAK1 fine-tunes the functions of AP2M in root cells. How the AP2M phosphorylation regulates endocytosis in plant cells and modulates root tropisms remains to be determined.

MATERIALS AND METHODS

Plant materials and growth conditions

Arabidopsis thaliana (L.) Heynh., accession Columbia-0, plants were used for all experiments. Arabidopsis seeds were surface sterilized by chlorine gas and sown on half-strength Murashige and Skoog ($\frac{1}{2}$ MS) solid plates (2.15 g/L MS salt [Duchefa], 10 g/L sucrose [Chem-Lab], 0.1 g/L myo-inositol [Sigma-Aldrich], 0.5 g/L MES [Duchefa], pH 5.7) with different concentration of agar as indicated. The plates were vernalized at 4°C under dark conditions for 3 days. Seeds were germinated and grown at 22°C and a 16 h light/8 h dark photoperiod for 5, 7, or 10 days, either vertically or horizontally, according to the experiments. For all vertical experiments, the plates contained 1% (w/v) agar and were tilted at about 15° from the vertical axis according the plate rack design in the growth room. For horizontal experiments, the plates contained 1.2% (w/v) agar (except in Supplemental Figure S5, 0.4%, 0.8%, and 1%) and were placed horizontally. The *aak1-1* (SALK_00168) mutant was obtained from the Arabidopsis Biological Resource Center. The transgenic Arabidopsis lines *pPIN2:PIN2-GFP/Col-0* (Adamowski et al., 2018), *pAP2M:AP2M-GFP/ap2m-2* (Yamaoka et al., 2013), *pAP2S:AP2S-*

GFP/ap2s (Fan et al., 2013), *p35S:GFP/Col-0* (Zhang et al., 2022), *ap2m-2* (Yamaoka et al., 2013), and *aux1-7* (Pickett et al., 1990) have been described previously.

Generation of constructs and transformation

For *pAAK1:AAK-GFP*, the promoter region (1873 bp) and the genomic DNA of *AAK1* (AT2G32850) were first cloned into the Gateway entry vectors *pDNORp4p1r* and *pDONR221*, respectively, with BP reactions, and then subcloned with *pDONR P2r-P3-GFP* into the binary vector *pK7m34GW* (Karimi et al., 2005) by a LR reaction. For AAK1OE, the *gAAK1-pDONR221* entry clone was subcloned into *pK7FWG2* (Karimi et al., 2002) by a LR reaction to generate the *p35S:gAAK1-GFP* construct. For *pAAK1:nlsGFP*, *pAAK1-pDNORp4p1r* was subcloned into the expression vector *pMK7S*NFm14GW* (Karimi et al., 2007). For *pAAK1:AAK1^{K57A}* and *pAAK1:AAK1^{D157A}*, the *pAAK1-pDNORp4p1r* and *gAAK1-pDONR221* entry clones were first subcloned into the *pH7m24GW* (Karimi et al., 2007) binary vector and then mutated by site-directed mutagenesis with the primers listed in Supplemental Table 1. For *pAP2M:AP2M*, the genomic DNA of *AP2M*, including its promoter region (2083 bp), was cloned into *pGGC000* and then further mutated by site-directed mutagenesis to generate the *pAP2M:AP2M^{T163A}-pGGC000*, *pAP2M:AP2M^{T163D}-pGGC000*, and *pAP2M:AP2M^{T163E}-pGGC000*. The entry clones were subcloned into the binary vector *pFASTRK-AG* with *pGG-A-LinkerIII-C* and *pGG-D-NOST-G* (Houbaert et al., 2018; Decaestecker et al., 2019) by the GoldenGate system (Karimi and Jacobs, 2021). The constructs were first transferred to the *Agrobacterium tumefaciens* C58C1 strain pMP90 and then transformed into Arabidopsis Col-0, *aak1-1*, or *ap2m-3* by floral dip.

For the CRISPR/Cas9 constructs, four and two gRNAs that target the first and the last exons of *AAK1* and the first exon of *AP2M* (AT5G46630), respectively, were designed with the ‘CCtop’ software (<https://cctop.cos.uni-heidelberg.de:8043/>). The four *AAK1* gRNA (Supplemental Table 1) were cloned into the entry vectors *pGG-C-AtU6-26-BbsI-ccdB-BbsI-D*, *pGG-D-AtU6-26-BbsI-ccdB-BbsI-E*, *pGG-E-AtU6-26-BbsI-ccdB-BbsI-F*, and *pGG-F-AtU6-26-BbsI-ccdB-BbsI-G*, and the two *AP2M* gRNAs (Supplemental Table 1) into *pGG-E-AtU6-26-BbsI-ccdB-BbsI-F* and *pGG-F-AtU6-26-BbsI-ccdB-BbsI-G*, according to the previously described protocol (Decaestecker et al., 2019). The CRISPR/Cas9 expression constructs were generated by assembling the *AAK1* gRNA and the *AP2M* gRNA entry clones with *pGG-A-linkerIII-E-C* and *pGG-A-linkerIII-E-G*, respectively, into the backbone vector *pFASTRK-Atcas9-AG* (Blomme et al., 2022) by the Golden Gate reaction. The expression constructs were transferred to the *Agrobacterium tumefaciens* C58C1 and then transformed into

Arabidopsis Col-0 by floral dip. For genotyping, the genomic DNA sequence of *AAK1* and *AP2M* of the transgenic plants were amplified by PCR with the primers listed in the Supplemental Table 1.

For protein purification, the constructs for GST-AP2M, GST-AP2A1, and GST-AP2S have been described previously (Liu et al., 2020). The MBP-AAK1 and GST-AP2M-T163 and GST-AP2M-T163A constructs were cloned into *pOPINM* and into *pOPINJ* by in-fusion cloning (Berrow et al., 2007), respectively, with the primers listed in Supplemental Table 1.

Root phenotype assays

For the root waving assay (Figure 1C), seedlings were grown vertically on ½MS plates with 1% (w/v) agar with a 15° tilted angle for 5 days. A wave was defined as a root turning angle of less than 120°. The waving numbers of individual roots were divided by their root length to obtain the waving number/cm ratio (Lanza et al., 2012).

Root horizontal assay

For the root horizontal assay, seedlings were grown on horizontal plates with 1.2% (w/v) agar for 7 days. The root penetration assay (Supplemental Figure S5) was carried out in plates containing 0.4%, 0.6% and 1% (w/v) agar and plants were grown horizontally. An arch root was defined as a root with more than half of it detached from the surface, whereas a wavy root as a root with more than half of it growing wavily along the surface and a curly root as a root with least one 360° turn on it.

Gravistimulation of plants

Five-day-old seedlings, light-grown vertically on ½MS medium, were gravistimulated by a 90° rotation in the vertical plane. The angle of the root tips deviating from the old gravity vector was measured 0 h, 3 h, 6 h, 9 h and 24 h after gravistimulation with the ImageJ software (<http://rsb.info.nih.gov/ij/>).

Protein purification

The MBP-AAK1, GST-AP2M, GST-AP2A1, GST-AP2S, GST-AP2M-T163, and GST-AP2M-T163A constructs were transformed into competent *Escherichia coli* BL21 (DE3) and the transformed cells were cultured in Luria-Bertani medium supplemented with 100 mg/mL carbenicillin at 37°C to an optical density of 0.6. Expression was induced by the addition of 0.2 mM isopropyl β-D-1-thiogalactopyranoside (IPTG) at 16°C overnight or 1 mM IPTG at

37°C for 3 h (fr GST-AP2M-T163 and GST-AP2M-T163A. Cells were harvested by centrifugation at 6,000g. For MBP-AAK1, cells were resuspended in lysis buffer (20 mM Tris-HCl, 200 mM NaCl, 1 mM EDTA, 1 mM dithiothreitol, 200 μM phenylmethylsulfonyl fluoride, protease inhibitors (Roche), pH 7.4) and lysed by sonication. MBP-AAK1 and GST-tagged proteins were purified with amylose resin (New England Biolabs) and with glutathione sepharose 4B GST-tagged protein purification resin (GE Healthcare), respectively, according to the standard manufacturers' protocols.

Liquid Chromatography with tandem mass spectrometry (LC-MS/MS) analysis of phospho-peptide detection

Peptides were redissolved in 20 μL loading solvent A (0.1% [v/v] trifluoroacetic acid in water/acetonitrile (98:2 [v/v])), of which 5 μL was injected for LC-MS/MS analysis on an Ultimate 3000 RSLC nano LC (Thermo Fisher Scientific) connected in-line to a Q Exactive mass spectrometer (Thermo Fisher Scientific). The peptides were first loaded on an in-house made trapping column [100 μm internal diameter (I.D.) × 20 mm, 5 μm beads C18 Repronil-HD (Dr. Maisch, Ammerbuch-Entringen, Germany)]. After the peptides had been flushed from the trapping column, they were separated on a 50 cm μPAC™ column with C18-encapped functionality (Pharmafluidics, Ghent, Belgium) kept at a constant temperature of 35°C. Peptides were eluted by a linear gradient from 98% (v/v) solvent A' (0.1% [v/v] formic acid in water) to 55% (v/v) solvent B' (0.1% [v/v] formic acid in water/acetonitrile, 20/80 [v/v]) in 30 min at a flow rate of 300 nL/min, followed by a 5 min wash reaching 99% (v/v) solvent B'.

The mass spectrometer was operated in data-dependent, positive ionization mode, automatically switching between MS and MS/MS acquisition for the five most abundant peaks in a given MS spectrum. The source voltage was 3.2 kV and the capillary temperature 275°C. One MS1 scan (m/z 400–2,000, AGC target 3×10^6 ions, maximum ion injection time 80 ms), acquired at a resolution of 70,000 (at 200 m/z), was followed by up to five tandem MS scans (resolution 17,500 at 200 m/z) of the most intense ions fulfilling predefined selection criteria (AGC target 5×10^4 ions, maximum ion injection time 80 ms, isolation window 2 Da, fixed first mass 140 m/z , centroid as spectrum data type, intensity threshold $1.3 \times E^4$, one exclusion of unassigned, >8 positively charged precursors, peptide match preferred, 'exclude isotopes' on, dynamic exclusion time 12 s). The higher-energy collision dissociation was set to 25% of the normalized collision energy and the polydimethylcyclsiloxane background ion at 445.120025 Da was used for internal calibration (lock mass). The raw files were processed with the MaxQuant software (version 1.6.10.43) (Cox and Mann, 2008), and searched with the built-in

Andromeda search engine against the Araport11plus database that contains crap sequences, e.g., tags, keratins, and trypsin. Search parameters can be found in the Supplemental Dataset 1.

***In vitro* kinase assay**

Recombinant proteins were incubated in the kinase reaction buffer (50 mM Tris-HCl, pH 7.5, 100 mM NaCl, 10 mM MgCl₂, and 10 μM ATP) in the presence of 5 μCi [γ -³²P]-ATP (NEG502A001MC; Perkin-Elmer) at 25°C for 60 min. The reactions were terminated by adding NuPAGE LDS sample buffer (Invitrogen) and NuPAGE sample-reducing agent (Invitrogen), separated on 4-20% sodium dodecyl sulfate-polyacrylamide gel electrophoresis (SDS-PAGE), and stained with Coomassie Brilliant Blue. Gels were dried and radioactivity was detected by autoradiography on a photographic film with an FLA 5100 phosphor imager (Fujifilm).

Co-immunoprecipitation assay

For Co-IP in Arabidopsis, seeds were germinated and grown on ½MS. Ten-day-old seedlings were harvested and ground into powder with liquid nitrogen. The fine powder was resuspended in extraction buffer (50 mM Tris-HCl, pH 7.5, 150 mM NaCl, 0.5% [v/v] NP-40, and complete EDTA-free protease inhibitor cocktail [Roche]). The extracts were centrifuged at 18,000 × g at 4°C for 10 min. The supernatants were transferred to new 2-ml tubes and centrifuged for an additional 10 min. After centrifugation, the supernatants were incubated with GFP-trap magnetic agarose (Chromotek) at 4°C for 1 h. Beads were washed three times with 1 mL wash buffer (20 mM Tris-HCl, pH 7.5, 150 mM NaCl, 0.25% [v/v] NP-40) and then eluted with 80 μL elution buffer containing 1× NuPAGE™ LDS Sample Buffer (Thermo Fisher Scientific) and 1× NuPAGE® Reducing Agent (Thermo Fisher Scientific) and heated at 60°C for 10 min.

SDS-PAGE and Western Blotting

Total protein extracts were obtained by grinding the plant materials into a fine powder with liquid nitrogen. The powder was resuspended in extraction buffer (50 mM Tris-HCl, pH 7.5, 150 mM NaCl, 0.5% [v/v] NP-40, and complete EDTA-free protease inhibitor cocktail [Roche]). The extracts were centrifuged at 18,000 × g at 4°C for 10 min. The supernatants were transferred to new 2-ml tubes and centrifuged for an additional 10 min. The protein extracts were boiled in sample buffer (1× NuPAGE™ LDS sample buffer, 1× NuPAGE® Reducing Agent [Thermo Fisher Scientific]) for 10 min at 60°C and loaded on a 4-20% (w/v) Mini-PROTEAN® TGX™ Precast Protein Gels (Bio-Rad). The proteins were separated by

electrophoresis and blotted onto a membrane with trans-Blot Turbo Mini 0.2 μm Nitrocellulose Transfer Packs (Bio-Rad). Membranes were blocked overnight at 4°C in 5% (w/v) skimmed milk dissolved in 25 mM Tris-HCl (pH 8), 150 mM NaCl, and 0.05% (v/v) Tween20. The blots were then incubated at room temperature with the monoclonal α -GFP antibody (1:5000) (Miltenyi Biotec, 130-091-833), α -tubulin antibody (1:5000) (Sigma-Aldrich, T5168), and α -AAK1 antibody (1:5000). α -AAK1 antibody was a custom antibody generated by Eurogentec using the antigen: QRYGNSKMRENQKTA.

Quantitative RT-PCR

RNA was extracted from 7-day-old seedlings with the ReliaPrep™ RNA Miniprep Systems (Promega). Of purified RNA, 1 μg was amplified in a reverse transcriptase reaction with the qScript XLT 1-Step RT-PCR Kit (Quantabio). Subsequently, qPCR was run with the SYBR Green master mix (Roche) using gene-specific primers designed to amplify *AP2M*. *ACTIN2* was used as the normalization reference. Primers are listed in the Supplementary Table S1.

Chemical treatments

For subcellular localization of AAK1-GFP, 4-day-old *pAAK1:AAK1-GFP/aak1-1* seedlings were treated with 50 μM BFA (50 mM stock in dimethyl sulfoxide; Sigma-Aldrich) and 2 μM (*N*-(3-triethylammoniumpropyl)-4-(6-(4-(diethylamino) phenyl) hexatrienyl) pyridinium dibromide) (FM4-64; 2 mM stock in purified water; Invitrogen) in $\frac{1}{2}$ MS liquid medium without sucrose for 30 min prior to confocal imaging. For FM4-64 uptake experiments, 4-day-old seedlings were incubated in $\frac{1}{2}$ MS liquid medium without sucrose containing 2 M FM4-64 for 10 min prior to confocal imaging. For PIN2-GFP recycling experiments, 5-day-old seedlings were pretreated with cycloheximide (CHX) (50 μM , 1 h) followed by a co-treatment with CHX (50 μM) and BFA (50 μM) in $\frac{1}{2}$ MS liquid medium for 30 min. Seedlings were subsequently washed with medium containing CHX (50 μM) for 100 min.

Confocal microscopy and image analysis

All confocal images were acquired with a Leica SP8X confocal microscope with the gating system (0.3-6 ns) application for autofluorescence removal. GFP, FM4-64, and AFCS were excited by white laser. The excitation and detection window settings were: GFP, 488/500-530 nm; FM4-64, 515/570–670 nm; and AFCS, 635/655-755 nm. For FM4-64 uptake and PIN2-GFP internalization and recycling experiments, images were captured on the cell cortex layer of the epidermal cells at the root transition zone with a laser configuration without

saturated signals. The fluorescent PM intensity and intracellular space were measured with ImageJ for the quantification of the FM4-64 uptake and the PIN2-GFP signal. PM and intracellular space of individual cells were selected with a brush tool size of 5 pixels and the polygon selection tool and histograms of pixel intensities were generated. The average intensity of the top 100 highest pixels based on the histogram for both the PM and the intracellular space was used to calculate the cytoplasm/PM ratios (Ortiz-Morea et al., 2016; Liu et al., 2020). BFA body size and BFA body number analyses were measured as described previously (Luo et al., 2015). The polarity of PIN2-GFP signals was calculated by determination of mean values of defined PM-areas at the apical and lateral side of root epidermis or at the basal and lateral side of root cortex cells as described previously (Kakar et al., 2013). For the AFCS experiments, the fluorescence intensities from the region of interest (ROI) of a maximum projected stack of eight slices, 1.5 μm apart, were quantified and normalized to the area as previously described (Irani et al., 2014). For kymographs of AAK1-GFP and AP2S-GFP, endocytic foci *in vivo* were measured with an Ultra View Vox Spinning disc confocal imaging system (PerkinElmer), running on the Volocity software package mounted on an Eclipse Ti inverted microscope (Nikon) with a Plan Apo Lambda 100 \times oil; numerical aperture, 1.45) corrected lens and third-generation perfect focus system (PFSIII) for Z-drift compensation. Time series were acquired at two time points per second intervals for 2 min. Excitation was done with a solid-state 488 nm diode-pumped solid-state laser (50 mW) (Perkin Elmer). Kymographs were generated with a line thickness of 3.

Statistical analysis

All statistical analyses and graph generations were done with the GraphPad Prism v.8 software. Kruskal-Wallis one-way analysis of variance (ANOVA) with Dunnett's multiple comparisons was applied for the statistical tests. The relative frequency distribution histograms were created by means of the frequency distribution function in column analyses with bin width of 0.04 for *aak1-1*, *aak1-2*, AAK1OE, and *pAP2M:AP2M^{T163A}/ap2m-3* and 0.05 for *ap2m-2*, *ap2m-3*, and *pAP2M:AP2M/ap2m-3*, automatically chosen by GraphPad Prism based on best-fit. The curve fitting was analyzed by nonlinear regression in XY analyses with a distribution function fitting better with the frequency distribution according to the least $S_{y,x}$ value for goodness-of-fit.

Accession Numbers

Sequence data from this article can be found in the GenBank/EMBL/TAIR data libraries under the following accession numbers. Arabidopsis genes: *AAK1* (AT2G32850), *AP2M*

(AT5G46630), *AP2S* (AT1G47830), *NECAP-1* (AT3G58600), *PIN2* (AT5G57090). For phylogenetic analysis and amino acid alignment of human genes: *AAK1* (Q2M2I8), *BIKE* (Q9NSY1), *GAK* (O14976), *AP2M1* (Q96CW1). For yeast genes: *ALK1* (P43633), *ENV7* (Q12003). For mouse genes: *AAK1* (Q3UHQ0), *BIKE* (Q91Z96), *GAK* (Q99KY4), *MPSK* (O88697). For fly genes: *PSK* (Q9VI84), *NAK* (Q9VJ30), *Auxilin* (Q9VMY8). For nematode genes: *gakh-1* (Q20483), *sel-5* (G5ECQ3). For Chlamydomonas gene: CR07G02400 (A0A2K3DJ59). For Brassica genes BR03G16570 (M4E2C4), BR05G11370 (M4CMW4). For maize genes: ZM02G25990 (A0A1D6Q3X3), ZM05G32400 (A0A1D6HBX6); ZM04G17600 (K7U1D6), ZM08G11310 (A0A3L6DLW1). For rice genes: OS09G10720 (XP_015612326.1), OS02G37880 (XP_015627128). For soybean genes: GM08G15921 (K7L6T7), GM15G42460 (I1MJK2). For tomato gene: SL01G074010 (XP_004229357).

Supplemental data

The following materials are available in the online version of this article.

Supplemental Figure S1 Sequence conservation and domain organization of AAK1.

Supplemental Figure S2 Phosphorylation of AP2-M.

Supplemental Figure S3 Expression and localization of AAK1 in Arabidopsis.

Supplemental Figure S4 Phenotypes of *aak1* and *ap2m* mutants.

Supplemental Figure S5 Root penetration assay and root behavior.

Supplemental Figure S6 The kinase-dead AAK1 did not rescue the root phenotype of *aak1-1*.

Supplemental Figure S7 The phospho-mimic forms of AP2M rescue the root behavior of *aak1-1*.

Supplemental Figure S8 FM4-64 uptake

Supplemental Table S1 Primer list.

Supplemental Movie 1 Subcellular localization of AAK1-GFP in root and cotyledon cells.

Supplemental Dataset 1 Phosphopeptide analysis of AP2M-T163A peptide

Acknowledgments

We thank I. Hara-Nishimura (Konan University, Japan) and J. Lin (Beijing Forestry University, China) for providing published materials, L. Sterck and S.M. Kao (VIB-UGent, Belgium) for help with phylogenetic analysis, X. Xu, D. Eeckhout and G. De Jaeger (VIB-UGent, Belgium)

for help with MS analyses and useful discussions, D. Van Damme and P. Grones (VIB-UGent, Belgium) for critical reading the manuscript, and M. De Cock for help in preparing it.

Funding

This work was supported by the Research Foundation-Flanders projects (G008416N, G0E5718N, and 3G038020 to E.R.). X.Z. and P.W. are indebted to the China Scholarship Council for predoctoral fellowships. L.D.V. received the post-doctoral fellowship of the Special Research Fund (Bijzonder Onderzoeksfonds, Ghent University).

Conflict of interest statement. The authors declare no competing interests.

Author contributions

W.S., X.Z. and E.R. conceived the project. W.S. did most of the work. P.W. generated the *ap2m-3* mutant and performed the kinetics of root gravitropism, qPCR analysis and BFA washout experiment. X.Z. isolated the *aak1-1* mutant and generated the AAK1OE and *pAAK1:nlsGFP* lines. L.D.V., and I.D.S. analyzed and interpreted the MS data. W.S. and E.R. wrote the manuscript. All authors revised the manuscript.

References

- Adamowski M, Narasimhan M, Kania U, Glanc M, De Jaeger G, Friml J** (2018) A functional study of AUXILIN-LIKE1 and 2, two putative clathrin uncoating factors in Arabidopsis. *Plant Cell* **30**: 700–716
- Agajanian MJ, Walker MP, Axtman AD, Ruela-de-Sousa RR, Serafin DS, Rabinowitz AD, Graham DM, Ryan MB, Tamir T, Nakamichi Y, et al** (2019) WNT activates the AAK1 kinase to promote clathrin-mediated endocytosis of LRP6 and establish a negative feedback loop. *Cell Reports* **26**: 79-93
- Baral A, Irani NG, Fujimoto M, Nakano A, Mayor S, Mathew MK** (2015) Salt-induced remodeling of spatially restricted clathrin-independent endocytic pathways in Arabidopsis root. *Plant Cell* **27**: 1297-1315
- Beacham GM, Partlow EA, Lange JJ, Hollopeter G** (2018) NECAPs are negative regulators of the AP2 clathrin adaptor complex. *eLife* **7**: e32242
- Berrow NS, Alderton D, Sainsbury S, Nettleship J, Assenberg R, Rahman N, Stuart DI, Owens RJ** (2007) A versatile ligation-independent cloning method suitable for high-throughput expression screening applications. *Nucleic Acids Res* **35**: e45

- Blomme J, Develtere W, Köse A, Arraiza Ribera J, Brugmans C, Jaraba-Wallace J, Decaestecker W, Rombaut D, Baekelandt A, Fernández Fernández ÁD, et al** (2022) The heat is on: a simple method to increase genome editing efficiency in plants. *BMC Plant Biol* **22**: 142
- Bolte S, Talbot C, Boutte Y, Catrice O, Read ND, Satiat-Jeunemaitre B** (2004) FM-dyes as experimental probes for dissecting vesicle trafficking in living plant cells. *J Microsc* **214**: 159-173
- Borner GHH, Antrobus R, Hirst J, Bhumbra GS, Kozik P, Jackson LP, Sahlender DA, Robinson MS** (2012) Multivariate proteomic profiling identifies novel accessory proteins of coated vesicles. *J Cell Biol* **197**: 141-160
- Chen X, Barg S, Almers W** (2008) Release of the styryl dyes from single synaptic vesicles in hippocampal neurons. *J Neurosci* **28**: 1894-1903
- Collins BM, McCoy AJ, Kent HM, Evans PR, Owen DJ** (2002) Molecular architecture and functional model of the endocytic AP2 complex. *Cell* **109**: 523-535
- Conner SD, Schmid SL** (2002) Identification of an adaptor-associated kinase, AAK1, as a regulator of clathrin-mediated endocytosis. *J Cell Biol* **156**: 921-929
- Conner SD, Schmid SL** (2003) Differential requirements for AP-2 in clathrin-mediated endocytosis. *J Cell Biol* **162**: 773-779
- Conner SD, Schroter T, Schmid SL** (2003) AAK1-mediated μ 2 phosphorylation is stimulated by assembled clathrin. *Traffic* **4**: 885-890
- Dason JS, Smith AJ, Marin L, Charlton MP** (2010) Vesicular sterols are essential for synaptic vesicle cycling. *J Neurosci* **30**: 15856-15865
- Decaestecker W, Buono RA, Pfeiffer ML, Vangheluwe N, Jourquin J, Karimi M, Van Isterdael G, Beeckman T, Nowack MK, Jacobs TB** (2019) CRISPR-TSKO: a technique for efficient mutagenesis in specific cell types, tissues, or organs in *Arabidopsis*. *Plant Cell* **31**: 2868-2887
- Dhonukshe P, Aniento F, Hwang I, Robinson DG, Mravec J, Stierhof Y-D, Friml J** (2007) Clathrin-mediated constitutive endocytosis of PIN auxin efflux carriers in *Arabidopsis*. *Curr Biol* **17**: 520-527
- Di Rubbo S, Irani NG, Kim SY, Xu Z-Y, Gadeyne A, Dejonghe W, Vanhoutte I, Persiau G, Eeckhout D, Simon S, et al** (2013) The clathrin adaptor complex AP-2 mediates endocytosis of BRASSINOSTEROID INSENSITIVE1 in *Arabidopsis*. *Plant Cell* **25**: 2986-2997

- Dietrich D, Pang L, Kobayashi A, Fozard JA, Boudolf V, Bhosale R, Antoni R, Nguyen T, Hiratsuka S, Fujii N, et al** (2017) Root hydrotropism is controlled via a cortex-specific growth mechanism. *Nat Plants* **3**: 17057
- Durham Brooks TL, Miller ND, Spalding EP** (2010) Plasticity of Arabidopsis root gravitropism throughout a multidimensional condition space quantified by automated image analysis. *Plant Physiol* **152**: 206-216
- Eapen D, Barroso ML, Ponce G, Campos ME, Cassab GI** (2005) Hydrotropism: root growth responses to water. *Trends Plant Sci* **10**: 44-50
- Fan L, Hao H, Xue Y, Zhang L, Song K, Ding Z, Botella MA, Wang H, Lin J** (2013) Dynamic analysis of *Arabidopsis* AP2 σ subunit reveals a key role in clathrin-mediated endocytosis and plant development. *Development* **140**: 3826-3837
- Galvan-Ampudia CS, Julkowska MM, Darwish E, Gandullo J, Korver RA, Brunoud G, Haring MA, Munnik T, Vernoux T, Testerink C** (2013) Halotropism is a response of plant roots to avoid a saline environment. *Curr Biol* **23**: 2044-2050
- Ghashghaie J, Brenckmann F, Saugier B** (1991) Effects of agar concentration on water status and growth of rose plants cultured in vitro. *Physiol Plant* **82**: 73-78
- Gupta-Rossi N, Ortica S, Meas-Yedid V, Heuss S, Moretti J, Olivo-Marin J-C, Israël A** (2011) The adaptor-associated kinase 1, AAK1, is a positive regulator of the Notch pathway. *J Biol Chem* **286**: 18720-18730
- Henderson DM, Conner SD** (2007) A novel AAK1 splice variant functions at multiple steps of the endocytic pathway. *Mol Biol Cell* **18**: 2698-2706
- Höning S, Ricotta D, Krauss M, Späte K, Spolaore B, Motley A, Robinson M, Robinson C, Haucke V, Owen DJ** (2005) Phosphatidylinositol-(4,5)-bisphosphate regulates sorting signal recognition by the clathrin-associated adaptor complex AP2. *Mol Cell* **18**: 519-531
- Houbaert A, Zhang C, Tiwari M, Wang K, de Marcos Serrano A, Savatin DV, Urs MJ, Zhiponova MK, Gudesblat GE, Vanhoutte I, et al** (2018) POLAR-guided signalling complex assembly and localization drive asymmetric cell division. *Nature* **563**: 574-578
- Irani NG, Di Rubbo S, Mylle E, Van den Begin J, Schneider-Pizoń J, Hniliková J, Šiša M, Buyst D, Vilarrasa-Blasi J, Szatmári AM, et al** (2012) Fluorescent castasterone reveals BRI1 signaling from the plasma membrane. *Nat Chem Biol* **8**: 583–589
- Irani NG, Di Rubbo S, Russinova E** (2014) In vivo imaging of brassinosteroid endocytosis in Arabidopsis. *In* MS Otegui, ed, *Plant Endosomes*, Ed 2014/08/15 Vol 1209. Springer, New York, pp 107-117

- Jackson AP, Flett A, Smythe C, Hufton L, Wettley FR, Smythe E** (2003) Clathrin promotes incorporation of cargo into coated pits by activation of the AP2 adaptor μ 2 kinase. *J Cell Biol* **163**: 231-236
- Jackson LP, Kelly BT, McCoy AJ, Gaffry T, James LC, Collins BM, Höning S, Evans PR, Owen DJ** (2010) A large-scale conformational change couples membrane recruitment to cargo binding in the AP2 clathrin adaptor complex. *Cell* **141**: 1220-1229
- Jacobsen AGR, Jervis G, Xu J, Topping JF, Lindsey K** (2021) Root growth responses to mechanical impedance are regulated by a network of ROS, ethylene and auxin signalling in *Arabidopsis*. *New Phytol* **231**: 225-242
- Kadlecova Z, Spielman SJ, Loeke D, Mohanakrishnan A, Reed DK, Schmid SL** (2016) Regulation of clathrin-mediated endocytosis by hierarchical allosteric activation of AP2. *J Cell Biol* **216**: 167-179
- Kakar K, Zhang H, Scheres B, Dhonukshe P** (2013) CLASP-mediated cortical microtubule organization guides PIN polarization axis. *Nature* **495**: 529-533
- Karimi M, Bleys A, Vanderhaeghen R, Hilson P** (2007) Building blocks for plant gene assembly. *Plant Physiol* **145**: 1183-1191
- Karimi M, De Meyer B, Hilson P** (2005) Modular cloning in plant cells. *Trends Plant Sci* **10**: 103-105
- Karimi M, Inzé D, Depicker A** (2002) GATEWAY™ vectors for *Agrobacterium*-mediated plant transformation. *Trends Plant Sci* **7**: 193-195
- Karimi M, Jacobs TB** (2021) GoldenGateway: A DNA Assembly Method for Plant Biotechnology. *Trends Plant Sci* **26**: 95-96
- Kelly BT, Graham SC, Liska N, Dannhauser PN, Höning S, Ungewickell EJ, Owen DJ** (2014) AP2 controls clathrin polymerization with a membrane-activated switch. *Science* **345**: 459-463
- Kim SY, Xu Z-Y, Song K, Kim DH, Kang H, Reichardt I, Sohn EJ, Friml J, Juergens G, Hwang I** (2013) Adaptor protein complex 2-mediated endocytosis is crucial for male reproductive organ development in *Arabidopsis*. *Plant Cell* **25**: 2970-2985
- Kirchhausen T, Owen D, Harrison SC** (2014) Molecular structure, function, and dynamics of clathrin-mediated membrane traffic. *Cold Spring Harb Perspect Biol* **6**: a016725
- Kitakura S, Vanneste S, Robert S, Löffke C, Teichmann T, Tanaka H, Friml J** (2011) Clathrin mediates endocytosis and polar distribution of PIN auxin transporters in *Arabidopsis*. *Plant Cell* **23**: 1920-1931

- Lanza M, Garcia-Ponce B, Castrillo G, Catarecha P, Sauer M, Rodriguez-Serrano M, Páez-García A, Sánchez-Bermejo E, TC M, Leo del Puerto Y, et al** (2012) Role of actin cytoskeleton in brassinosteroid signaling and in its integration with the auxin response in plants. *Dev Cell* **22**: 1275-1285
- Liu D, Kumar R, Claus LAN, Johnson AJ, Siao W, Vanhoutte I, Wang P, Bender KW, Yperman K, Martins S, et al** (2020) Endocytosis of BRASSINOSTEROID INSENSITIVE1 Is partly driven by a canonical Tyr-based motif. *Plant Cell* **32**: 3598-3612
- Loshchilov I, Del Dottore E, Mazzolai B, Floreano D** (2021) Conditions for the emergence of circumnutations in plant roots. *PLoS ONE* **16**: e0252202
- Luo Y, Scholl S, Doering A, Zhang Y, Irani NG, Di Rubbo S, Neumetzler L, Krishnamoorthy P, Van Houtte I, Mylle E, et al** (2015) V-ATPase activity in the TGN/EE is required for exocytosis and recycling in *Arabidopsis*. *Nat Plants* **1**: 15094
- Massol RH, Boll W, Griffin AM, Kirchhausen T** (2006) A burst of auxilin recruitment determines the onset of clathrin-coated vesicle uncoating. *Proc Natl Acad Sci USA* **103**: 10265-10270
- McMahon HT, Boucrot E** (2011) Molecular mechanism and physiological functions of clathrin-mediated endocytosis. *Nat Rev Mol Cell Biol* **12**: 517-533
- Men S, Boutté Y, Ikeda Y, Li X, Palme K, Stierhof Y-D, Hartmann M-A, Moritz T, Grebe M** (2008) Sterol-dependent endocytosis mediates post-cytokinetic acquisition of PIN2 auxin efflux carrier polarity. *Nat Cell Biol* **10**: 237-244
- Mergner J, Frejno M, List M, Papacek M, Chen X, Chaudhary A, Samaras P, Richter S, Shikata H, Messerer M, et al** (2020) Mass-spectrometry-based draft of the *Arabidopsis* proteome. *Nature* **579**: 409-414
- Mettlen M, Chen P-H, Srinivasan S, Danuser G, Schmid SL** (2018) Regulation of clathrin-mediated endocytosis. *Annu Rev Biochem* **87**: 871-896
- Miao R, Wang M, Yuan W, Ren Y, Li Y, Zhang N, Zhang J, Kronzucker HJ, Xu W** (2018) Comparative analysis of *Arabidopsis* ecotypes reveals a role for brassinosteroids in root hydrotropism. *Plant Physiol* **176**: 2720-2736
- Mitsunari T, Nakatsu F, Shioda N, Love PE, Grinberg A, Bonifacino JS, Ohno H** (2005) Clathrin adaptor AP-2 is essential for early embryonal development. *Mol Cell Biol* **25**: 9318-9323
- Newton J, Murthy V** (2006) Measuring exocytosis in neurons using FM labeling. *J Vis Exp* **1**: 117

- Oliva M, Dunand C** (2007) Waving and skewing: how gravity and the surface of growth media affect root development in *Arabidopsis*. *New Phytol* **176**: 37-43
- Olusanya O, Andrews PD, Swedlow JR, Smythe E** (2001) Phosphorylation of threonine 156 of the $\mu 2$ subunit of the AP2 complex is essential for endocytosis in vitro and in vivo. *Curr Biol* **11**: 896-900
- Ortiz-Morea FA, Savatin DV, Dejonghe W, Kumar R, Luo Y, Adamowski M, Van den Begin J, Dressano K, Pereira de Oliveira G, Zhao X, et al** (2016) Danger-associated peptide signaling in *Arabidopsis* requires clathrin. *Proc Natl Acad Sci USA* **113**: 11028-11033
- Partlow EA, Baker RW, Beacham GM, Chappie JS, Leschziner AE, Holloper G** (2019) A structural mechanism for phosphorylation-dependent inactivation of the AP2 complex. *eLife* **8**: e50003
- Pelkmans L, Fava E, Grabner H, Hannus M, Habermann B, Krausz E, Zerial M** (2005) Genome-wide analysis of human kinases in clathrin- and caveolae/raft-mediated endocytosis. *Nature* **436**: 78-86
- Pickett FB, Wilson AK, Estelle M** (1990) The *aux1* mutation of *Arabidopsis* confers both auxin and ethylene resistance. *Plant Physiol* **94**: 1462-1466
- Richards DA, Guatimosim C, Betz WJ** (2000) Two endocytic recycling routes selectively fill two vesicle pools in frog motor nerve terminals. *Neuron* **27**: 551-559
- Ricotta D, Conner SD, Schmid SL, von Figura K, Höning S** (2002) Phosphorylation of the AP2 μ subunit by AAK1 mediates high affinity binding to membrane protein sorting signals. *J Cell Biol* **156**: 791-795
- Roth TF, Porter KR** (1964) Yolk protein uptake in the oocyte of the mosquito *Aedes aegypti* L. *J Cell Biol* **20**: 313-332
- Růžička K, Ljung K, Vanneste S, Podhorská R, Beckman T, Friml J, Benková E** (2007) Ethylene regulates root growth through effects on auxin biosynthesis and transport-dependent auxin distribution. *Plant Cell* **19**: 2197-2212
- Sorrell FJ, Szklarz M, Abdul Azeez KR, Elkins JM, Knapp S** (2016) Family-wide structural analysis of human Numb-associated protein kinases. *Structure* **24**: 401-411
- Taylor MJ, Perrais D, Merrifield CJ** (2011) A high precision survey of the molecular dynamics of mammalian clathrin-mediated endocytosis. *PLoS Biol* **9**: e1000604
- Tojo H, Nakamura A, Ferjani A, Kazama Y, Abe T, Iida H** (2021) A method enabling comprehensive isolation of *Arabidopsis* mutants exhibiting unusual root mechanical behavior. *Front Plant Sci* **12**: 646404

- Traub LM** (2009) Tickets to ride: selecting cargo for clathrin-regulated internalization. *Nat Rev Mol Cell Biol* **10**: 583-596
- Umeda A, Meyerholz A, Ungewickell E** (2000) Identification of the universal cofactor (auxilin 2) in clathrin coat dissociation. *Eur J Cell Biol* **79**: 336-342
- Van Gisbergen PAC, Esseling-Ozdoba A, Vos JW** (2008) Microinjecting FM4-64 validates it as a marker of the endocytic pathway in plants. *J Microsc* **231**: 284-290
- Vu LD, Stes E, Van Bel M, Nelissen H, Maddelein D, Inzé D, Coppens F, Martens L, Gevaert K, De Smet I** (2016). Up-to-date workflow for plant (Phospho) proteomics identifies differential drought-responsive phosphorylation events in maize leaves. *J Proteome Res* **15**: 4304-4317
- Wang P, Siao W, Zhao X, Arora D, Wang R, Eeckhout D, Leene JV, Kumar R, Houbaert A, De Winne N, et al** (2023) Adaptor protein complex interaction map in Arabidopsis identifies P34 as a common stability regulator. *Nat Plants* **9**: 355-371
- Willems P, Horne A, Van Parys T, Goormachtig S, De Smet I, Botzki A, Van Breusegem F, Gevaert K** (2019) The Plant PTM Viewer, a central resource for exploring plant protein modifications. *Plant J* **99**: 752-762
- Wrobel AG, Kadlecova Z, Kamenicky J, Yang JC, Herrmann T, Kelly BT, McCoy AJ, Evans PR, Martin S, Müller S, et al** (2019) Temporal ordering in endocytic clathrin-coated vesicle formation via AP2 phosphorylation. *Dev Cell* **50**: 494-508
- Xia L, Mar Marqués-Bueno M, Bruce CG, Karnik R** (2019) Unusual roles of secretory SNARE SYP132 in plasma membrane H⁺-ATPase traffic and vegetative plant growth. *Plant Physiol Biochem* **180**: 837-858
- Yamamoto C, Sakata Y, Taji T, Baba T, Tanaka S** (2008) Unique ethylene-regulated touch responses of *Arabidopsis thaliana* roots to physical hardness. *J Plant Res* **121**: 509
- Yamaoka S, Shimon Y, Shirakawa M, Fukao Y, Kawase T, Hatsugai N, Tamura K, Shimada T, Hara-Nishimura I** (2013) Identification and dynamics of *Arabidopsis* adaptor protein-2 complex and its involvement in floral organ development. *Plant Cell* **25**: 2958-2969
- Yoshinari A, Hosokawa T, Amano T, Beier MP, Kunieda T, Shimada T, Hara-Nishimura I, Naito S, Takano J** (2019) Polar localization of the borate exporter BOR1 requires AP2-dependent endocytosis. *Plant Physiol* **179**: 1569-1580
- Zhang C, Lauster T, Tang W, Houbaert A, Zhu S, Eeckhout D, De Smet I, De Jaeger G, Jacobs TB, Xu T, et al** (2022) ROPGAP-dependent interaction between

AAK1 regulates root tropic growth in Arabidopsis

brassinosteroid and ROP2-GTPase signaling controls pavement cell shape in *Arabidopsis*. *Curr Biol* **32**: 518-531

Zhang Y, Friml J (2020) Auxin guides roots to avoid obstacles during gravitropic growth. *New Phytol* **225**: 1049-1052

Zulawski M , Braginets R , Schulze WX (2013) PhosPhAt goes kinases—searchable protein kinase target information in the plant phosphorylation site database PhosPhAt. *Nucleic Acids Res* **41**: D1176–D1184

AAK1 regulates root tropic growth in Arabidopsis

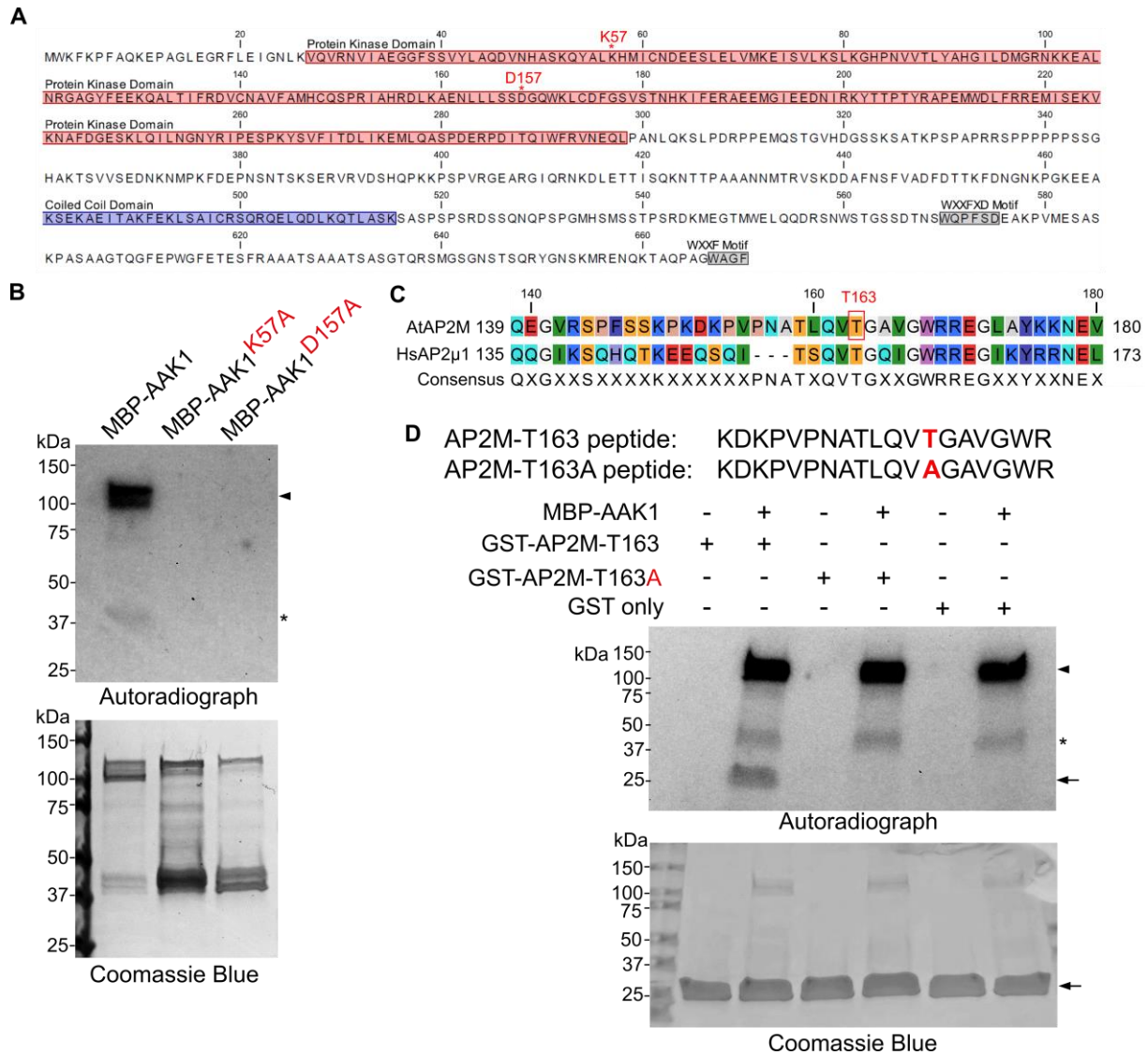


Figure 1 Arabidopsis AAK1 is an active kinase and phosphorylates AP2M on Thr-163 *in vitro*. A, Sequence and domain structures of Arabidopsis AAK1. The conserved lysine (K57) and aspartate (D157) that are important for nucleotide binding and catalysis are indicated. WXXFXD and WXXF are adaptin binding motifs. B, *In vitro* kinase assay with isotope labeling. The MBP-AAK1 fusion protein can autophosphorylate *in vitro* when incubated with [³²P]-γ-ATP, whereas the kinase-dead versions of AAK1, MBP-AAK1^{K57A}, and MBP-AAK1^{D157} had no autophosphorylation activity. C, Amino acid alignment of Arabidopsis AP2M and human AP2μ1. The threonine (T) phosphorylation site at position 156 in human AP2μ1 is conserved in the Arabidopsis AP2M at position 163 (T163). D, *In vitro* kinase assay of the AP2M GST-tagged peptide containing Thr-163 (AP2M-T163) and the GST-tagged mutant peptide, in which the Thr-163 was substituted with alanine (AP2M-T163A). MBP-AAK1 was used as kinase. The sequences of the short peptides (19 amino acids) are presented on the top. The GST protein was used as negative control. Arrowheads and asterisks in (B) and (D) indicate the autophosphorylation signal of MBP-AAK1 and nonspecific signals, respectively. Arrows in (D) indicate the size of the GST-AP2M-T163, GST-AP2M-T163A and GST.

AAK1 regulates root tropic growth in Arabidopsis

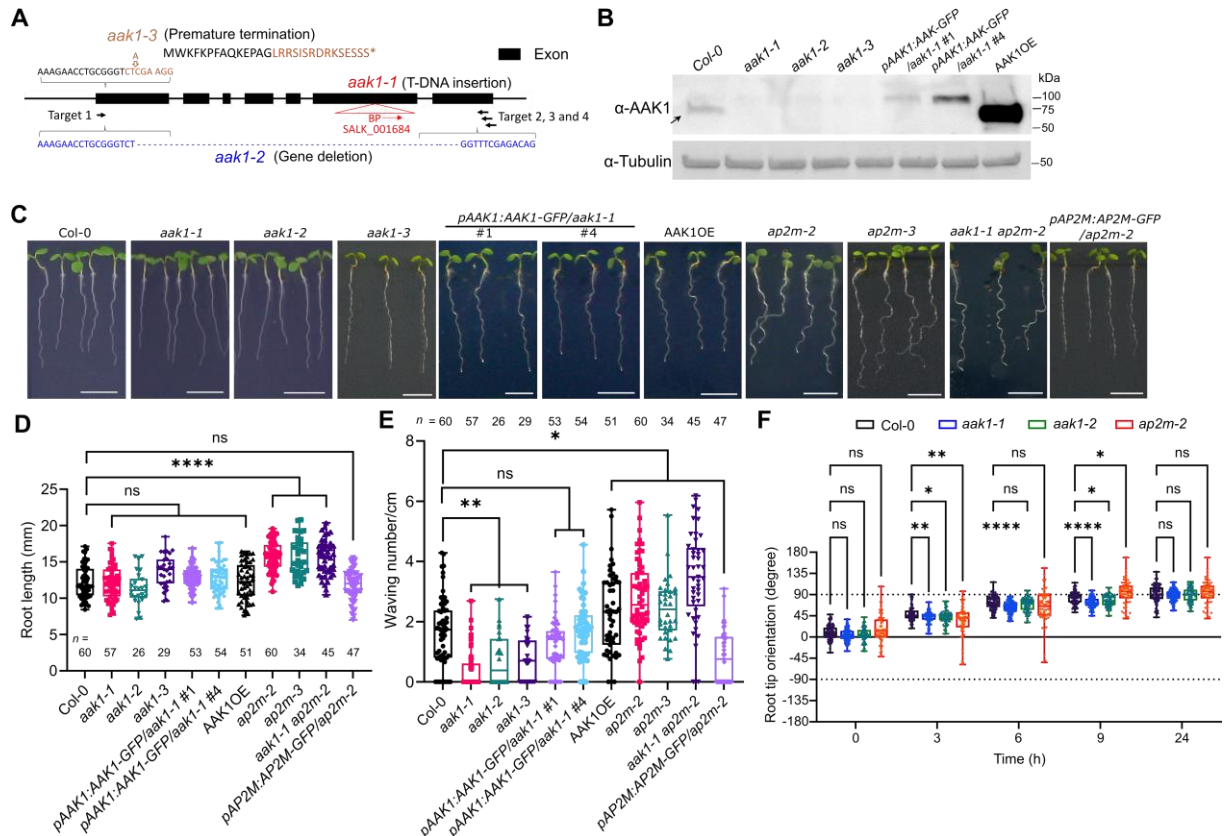


Figure 2 AAK1 and AP2M regulate root waving and gravitropism in Arabidopsis. **A**, Schematic representation of different *aak1* mutant alleles generated in this study. The locations of guide RNAs (gRNAs, black arrows) targeting the AAK1 locus is indicated. BP and Targets mark the T-DNA left border primer and the gDNA targeting sites, respectively. **B**, Immunoblot analysis of AAK1 protein levels in the wide type (Col-0), *aak1-1*, *aak1-2*, *aak1-3* mutants, *pAAK1:AAK1-GFP/aak1-1* (lines #1 and #4), and the AAK1 overexpression line (*p35S:AAK1-GFP/Col-0*, AAK1OE) with α -AAK1 antibody. Tubulin detected with α -tubulin antibody was used as a loading control. The arrow indicates the endogenous AAK1. **C**, Root phenotypes of 5-day-old seedlings of Col-0, *aak1-1*, *aak1-2*, *aak1-3* mutants, *pAAK1:AAK1-GFP/aak1-1* (lines #1 and #4), AAK1OE, and *ap2m-2* and *ap2m-3* mutants. Scale bar, 5 mm. **D**, Primary root length of each genotype as shown in (C). **E**, Root waving assay of each genotype as shown in (C). The root waviness was determined as the number of waves per root length. Three independent experiments were combined (D and E). **F**, Kinetics of the gravitropic bending of root tips of wild type, *aak1-1*, *aak1-2* and *ap2m-2* plotted against time after gravistimulation. Five-day-old seedlings grown vertically on medium were gravistimulated by 90° rotation. Three independent experiments were combined, each with 20-30 roots per genotype in each experiment. Error bars indicate the standard errors. *n*, number of roots (D-F). * $P \leq 0.05$, ** $P \leq 0.01$, *** $P \leq 0.001$ **** $P \leq 0.0001$ [one-way ANOVA tests in (D and E) and two-way ANOVA test in (F)], ns, not significant.

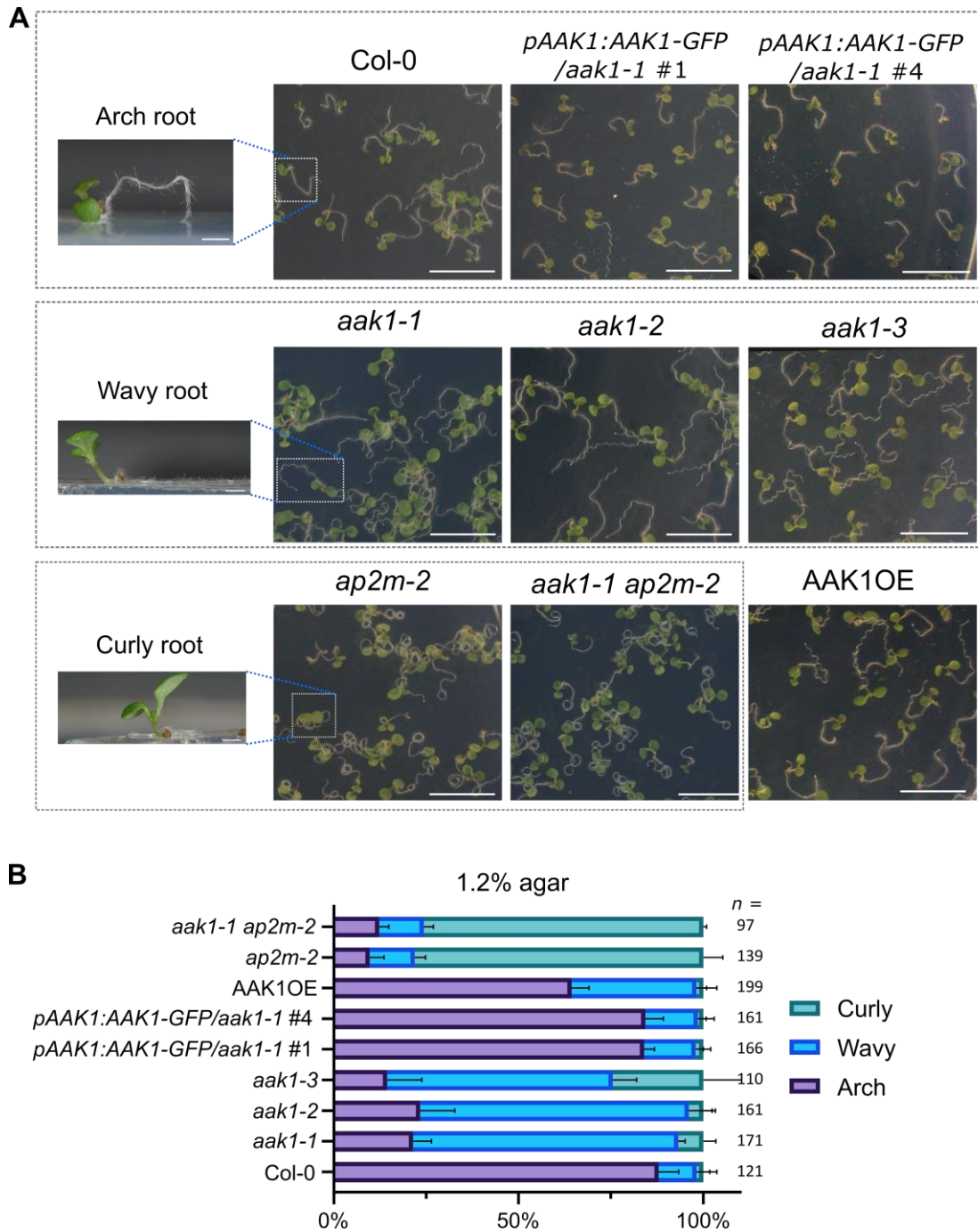


Figure 3 The primary roots of *aak1* and *ap2m* mutants exhibited distinct behaviors when grown on a surface of impenetrable agar. A, Representative images showing the root behavior (arch, wavy, and curly roots, as shown in the insets) of 7-day-old seedlings of wide type (Col-0), *aak1-1*, *aak1-2*, *aak1-3* mutants, *pAAK1:AAK1-GFP/aak1-1* (lines #1 and #4), the AAK1 overexpression line (*p35S:AAK1-GFP/Col-0*, AAK1OE), *ap2m-2* and *aak1-1 ap2m-2* mutants grown horizontally on 1.2% agar-containing medium. The genotypes exhibiting the same root behavior were grouped in dashed rectangles. Scale bars, 1 cm. B, Quantification of the root behavior of each genotype as in (A). Three independent experiments were combined. *n*, number of roots analyzed. Error bars represent the standard error (SE) of the three replicates.

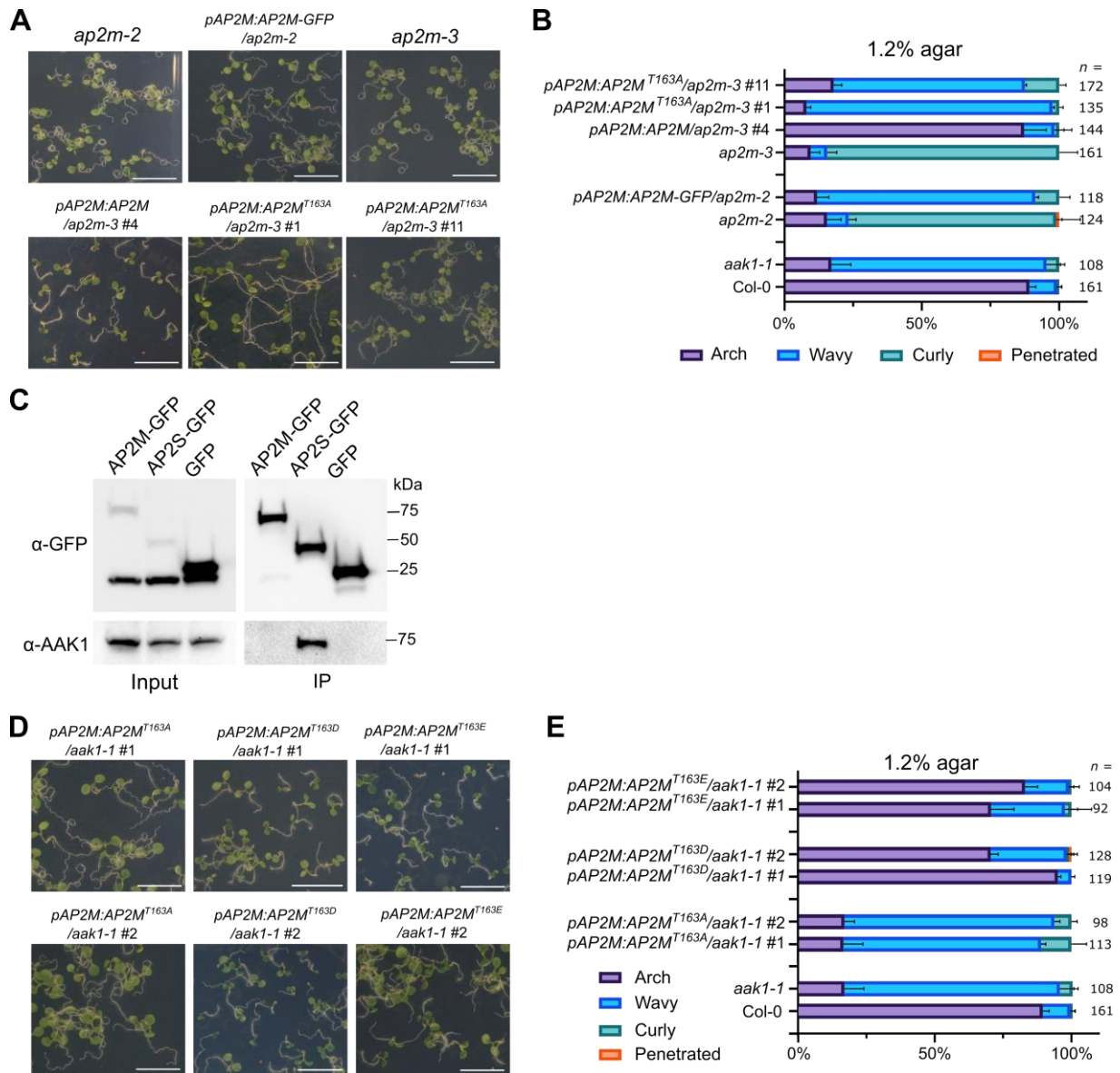


Figure 4 AP2M phosphorylation on Thr-163 by AAK1 regulates root behavior. A, Representative images of the root horizontal assay examining the root behavior of 7-day-old seedlings of *ap2m-2*, *ap2m-3*, and the complemented lines with different AP2M versions, *pAP2M:AP2M-GFP/ap2m-2*, *pAP2M:AP2M/ap2m-3* (line #4), and *pAP2M:AP2M^{T163A}/ap2m-3* (lines #1 and #11). T3 generation seedlings homozygous for the transgenes were analyzed. B, Quantification of the root behavior of each genotype as in (A). *Col-0* and *aak1-1* were used as control. Three independent experiments were combined. C, Co-immunoprecipitation (Co-IP) assay in *pAP2M:AP2M-GFP/ap2m-2* (AP2M-GFP) and *pAP2S:AP2S-GFP/ap2s* (AP2S-GFP) Arabidopsis plants. AP2M-GFP and AP2S-GFP were pulled down with GFP-trap beads. Endogenous AAK1 was detected with α -AAK1 antibody. The *p35S:GFP* (GFP) transgenic Arabidopsis plants were used as a negative control. Experiments were repeated twice with similar results. One representative experiment is presented. D, Representative images of the root horizontal assay on 7-day-old seedlings of *aak1-1* expressing the phospho-mimic AP2M (*pAP2M:AP2M^{T163D}/aak1-1* and *pAP2M:AP2M^{T163E}/aak1-1*) and the phospho-null AP2M (*pAP2M:AP2M^{T163A}/aak1-1*). Two independent T2 lines for each construct were analyzed. Seedlings (homozygous or heterozygous for the transgenes) were chosen based on fluorescent seed selection. E, Quantification of the root behavior of each genotype as in (D). Three independent experiments were combined. The *Col-0* and *aak1-1* were used as controls and were the same as in (B) because the experiments were done together. Error bars in (B) and (D) represent the standard error (SE) of the three replicates. *n*, number of roots. Scale bar, 1 cm (A and D).

AAK1 regulates root tropic growth in Arabidopsis

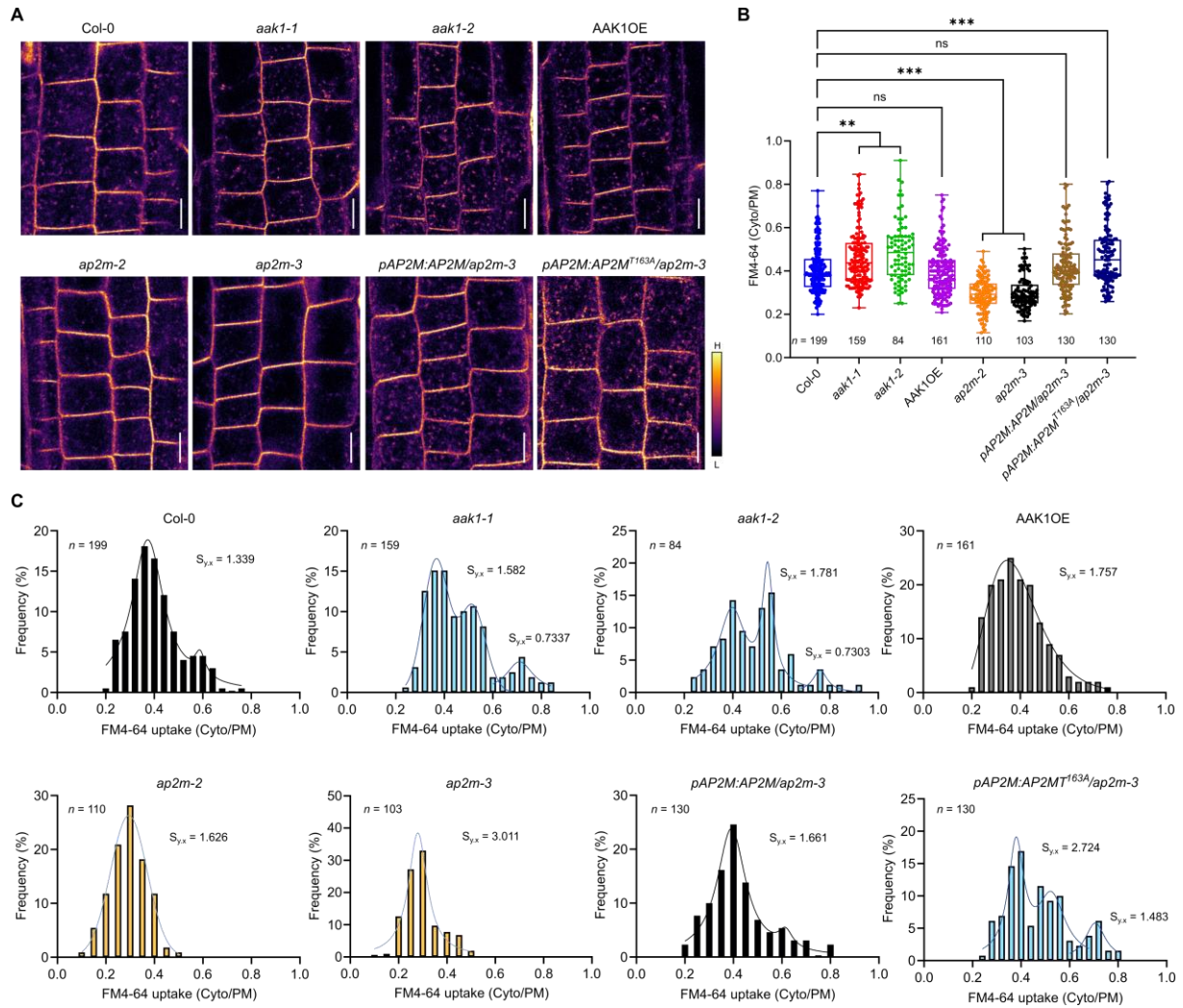


Figure 5 Phosphorylation of AP2M by AAK1 affects FM4-64 endocytosis. **A**, FM4-64 uptake in wild type (Col-0), *aak1-1*, *aak1-2*, the AAK1 overexpression line (*p35S:AAK1-GFP/Col-0*, AAK1OE), *ap2m-2*, *ap2m-3*, *pAP2M:AP2M/ap2m-3* (line #4), and *pAP2M:AP2M^{T163A}/ap2m-3* (line #1). Five-day-old root epidermal cells were imaged after staining with FM4-64 (2 μ M) for 10 min. Scale bars, 10 μ m. **B**, Relative cytoplasmic (Cyto) to plasma membrane (PM) fluorescence intensity ratio of FM4-64 of images in (A). ** $P \leq 0.01$, *** $P \leq 0.001$ (Kruskal-Wallis non-parametric one-way ANOVA test); ns, not significant. **C**, Frequency distribution graphs showing the ranges of the FM4-64 uptake in the root epidermal cells of the different genotypes in (B). The bin widths for best-fit were set at 0.04 for Col-0, *aak1-1*, *aak1-2*, AAK1OE, and *pAP2M:AP2M^{T163A}/ap2m-3* (line #1) and at 0.05 for *ap2m-2*, *ap2m-3*, and *pAP2M:AP2M/ap2m-3* (line #4) by GraphPad Prism. The curves were fitted by nonlinear regression with either Gaussian, Lorentzian, or Lognormal functions, according to the least standard deviation of the residuals ($S_{y,x}$) values for goodness-of-fit. *n*, number of cells analyzed (B and C).

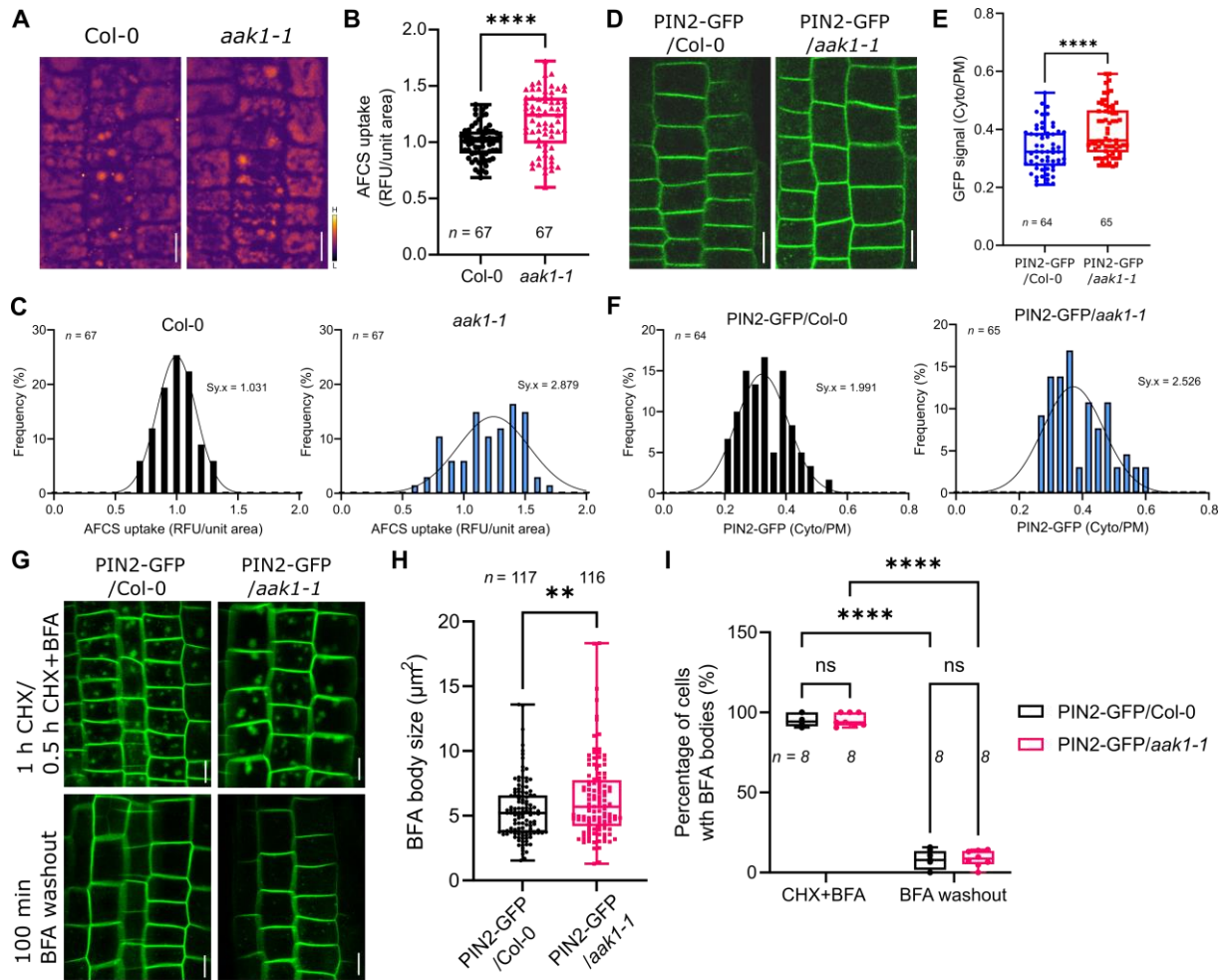


Figure 6 AAK1 regulates endocytosis of BRI1 and PIN2. A, Alexa Fluor 647-castasterone (AFCS) uptake in the root epidermal cells of 4-day-old Col-0 and *aak1-1*. Roots were pulsed with AFCS (30 μ M) for 40 min, washed, and then chased for 20 min before imaging. B, Quantification of AFCS fluorescence intensity in the vacuoles of the root cells of Col-0 and *aak1-1*. RFU, relative fluorescence units. **** $P \leq 0.0001$ (Welch's *t* test). *n*, number of unit area. C, Frequency distributions showing the ranges of the AFCS uptake in the root epidermal cells of Col-0 and *aak1-1*. The bin widths were set to 0.1. The curves were fitted by nonlinear regression with the Gaussian function for the least standard deviation of the residuals ($S_{y,x}$) value. *n*, number of unit area. D, Confocal images of *pPIN2:PIN-GFP* in the root epidermal cells of 5-day-old Col-0 and *aak1-1* seedlings. E, Relative cytoplasmic (Cyto) versus plasma membrane (PM) fluorescence intensity of PIN2-GFP of images in (D). *n*, number of cells. F, Frequency distributions showing the ranges of the Cyto/PM ratio of PIN2-GFP in the root epidermal cells of Col-0 and *aak1-1*. The bin widths were set to 0.03. G, Accumulation of PIN2-GFP in the root cells of 5-day-old wild type and *aak1-1* after Brefeldin A (BFA) treatment and after BFA washout. Seedlings were pretreated with cycloheximide (CHX) (50 μ M, 1 h) followed by a co-treatment with CHX (50 μ M) and BFA (50 μ M) for 30 min. Seedlings were washed with media containing CHX (50 μ M) and imaged 100 min after the wash. H, BFA body sizes before the washout shown in (G). *n*, number of BFA bodies. I, Percentage of BFA body-containing cells in PIN2-GFP seedlings before and after BFA washout shown in (G). *n*, number of roots. ** $P \leq 0.01$, **** $P \leq 0.0001$ [Welch's *t* test (E and H) and two-way ANOVA test (I)], ns, not significant. Scale bars, 10 μ m (A, D and G).